Constraining burial history and petroleum charge in exhumed basins: new insights from the Illizi Basin, Algeria

Kara L. English

Petroceltic International Plc, 3 Grand Canal Plaza, Grand Canal Street Upper, Dublin 4, Ireland.

E-mail: kara.english@yahoo.ca

Jonathan Redfern

School of Earth, Atmospheric and Environmental Sciences, University of Manchester, Williamson Building, Oxford Road, Manchester, M13 9PL, United Kingdom; E-mail: jonathan.redfern@manchester.ac.uk

Dermot V. Corcoran

Petroceltic International Plc, 3 Grand Canal Plaza, Grand Canal Street Upper, Dublin 4, Ireland.

E-mail: corcoran.diarmuid@gmail.com

Joseph M. English

Petroceltic International Plc, 3 Grand Canal Plaza, Grand Canal Street Upper, Dublin 4, Ireland.

E-mail: joseph.english@petroceltic.com

Rachida Yahia Cherif

Direction Coordination Groupe Associations – Sonatrach, Djenane El-Malik, Hydra, Alger, Algérie (Algeria); E-mail: Rachida.Yahiacherif@Sonatrach.dz

Main text word count = 8472

Abstract word count = 268

Number of tables = 6

Number of figures = 17

References = 105

Number of appendices = 0

Data Repository = No

Corresponding author = Kara English

VITAE

Kara L. English - Petroceltic International Plc, 3 Grand Canal Plaza, Grand Canal Street Upper, Dublin 4, Ireland; kara.english@yahoo.ca

Kara English is a chartered petroleum geologist currently completing her Ph.D. at the University of Manchester, England. She received her B.Sc. in geology from the University of Victoria, Canada (2004). She has over 10 years' experience in the petroleum industry, and has previously worked for EnCana Corporation and Petroceltic International. Her research interests include basin modelling, sedimentology, sandstone diagenesis and the impact of exhumation on petroleum systems analysis. She currently works with the Petroleum Affairs Division in the Department of Communications, Energy and Natural Resources in Dublin, Ireland.

Jonathan Redfern – North Africa Research Group, School of Earth, Atmospheric and Environmental Sciences, University of Manchester, Oxford Road, Manchester, M13 9PL, United Kingdom; jonathan.redfern@manchester.ac.uk

Jonathan Redfern obtained his B.Sc. degree from the University of London, Chelsea College, in 1983, and a Ph.D. from Bristol University, United Kingdom, in 1989. He worked in the oil industry for 12 years, initially with Fina in the North Sea, southeast Asia, and Libya, and subsequently with Hess as Chief Geologist in Indonesia. He is a Professor and Head of the Basin Studies, Petroleum Geoscience and Engineering Group at the University of Manchester and leads the North Africa Research Group, founded in 2000, which undertakes field and subsurface analysis across the region, sponsored by leading oil companies. His main research interests are in basin analysis, hydrocarbon systems, and continental and glacial sedimentology.

Dermot V. Corcoran – Petroceltic International Plc, 3 Grand Canal Plaza, Grand Canal Street Upper, Dublin 4, Ireland; corcoran.diarmuid@gmail.com

Dermot Corcoran is an exploration consultant with over 30 years' experience in the hydrocarbon sector. He received a B.Sc. degree (Geology) in 1980 and a M.Sc. degree (Applied Geophysics) in 1981 from the National University of Ireland (Galway). He was awarded a Ph.D. degree by Trinity College Dublin in 2005 and he has previously worked for extended periods with ExxonMobil, Statoil and Petroceltic International Plc. He currently works with Petrogen Energy Services Ltd.

Joseph M. English - Petroceltic International Plc, 3 Grand Canal Plaza, Grand Canal Street Upper, Dublin 4, Ireland; jenglish@petroceltic.com

Joe English is the chief geologist at Petroceltic International. He received his B.A. in geology from Trinity College, Dublin, Ireland (2001) and his Ph.D. from the University of Victoria, Canada (2004). He has previously worked for Encana Corporation and Nexen Inc., and is a chartered geologist under the Geological Society of London. His research interests include geomechanics, tectonics, structural geology, and basin analysis, and he is a previous winner of AAPG's Cam Sproule Memorial Award.

Rachida Yahia Cherif - Sonatrach, Djenane El-Malik, Hydra, Alger, Algérie (Algeria); rachida.yahiacherif@sonatrach.dz

Rachida Yahia Cherif (née Kherif) is a structural geologist at Sonatrach Exploration and Production. She received her degree in structural geology from the University of Science and Technology Houari Boumediene in Bab Ezzouar, Algeria. She worked for 3 years as a structural geology instructor at the Higher School in Vieux Kouba, Algeria, and has over 15 years' experience in Exploration and Production at Sonatrach. Her research interests include tectonics, structural geology, and basin analysis.

ACKNOWLEDGMENTS

We thank Petroceltic International, Sonatrach and Enel, for sponsoring this study and granting permission for publication. We gratefully acknowledge generous donations of the *Genesis* and *HeFTy* software for this research. This paper benefitted from discussions and contributions from Peter Rowbotham, Jenny Garnham, Richard Baker, Ciaran Nolan, Kevin Isaac, Remi Fontaine, Eloi Dolivo, Sean McDade, Brian O'Cathain, Norman Oxtoby, Jonathan Hunter, Tony Cave, Toyoki Nishibayashi, Djamila Daoudi, Sebastien Lüning, David Loydell, Lorraine B. Eglinton, Geoff Probert, Richard Dixon, Jake Hossack, Julian Moreau, Ian Duddy, and Susan Johnson. We also thank Ken Peters for constructive feedback, which helped to improve the quality of this work.

ABSTRACT

Intracratonic sag basins commonly have relatively simple tectonic histories; however, later tectonic activity involving exhumation can make reconstructing the burial history a challenging task. This is important because the relative timing of hydrocarbon generation and trap formation can be a key factor in risk assessment. If trap formation post-dates peak hydrocarbon generation, exploration plays are typically downgraded. Mechanisms for charge in such exhumed basins are a critical factor for understanding exploration risk. This study utilises data collected from an Ordovician multi-Tcf gas-condensate field in the Illizi Basin of Algeria to document the charging of a trap formed, or modified, during exhumation of the basin following maximum burial. Integrated analysis of sonic compaction data, thermal history indicators and stratigraphic insights has been used to constrain the burial and thermal history of the region. Hydrocarbon generation in the lower Silurian source rock is interpreted to have occurred during the Carboniferous (prior to Hercynian exhumation) and during Late Cretaceous–early Eocene maximum burial (prior to Eocene exhumation). Structural reconstructions indicate the field was initially located on the southern flank of a long-lived intra-basinal Paleozoic paleohigh, and that the large low-relief structural closure that defines the present-day accumulation formed as a result of northward tilting of the Illizi Basin during Eocene uplift of the Hoggar Massif. The study demonstrates that the timing of trap formation at the Ordovician field post-dates the main local hydrocarbon generation events within the basin, suggesting that alternative hydrocarbon charge mechanisms are required. This study indicates considerable potential to charge up-dip traps on the flanks of exhumed petroliferous basins via re-distribution of the pre-existing hydrocarbons within the basin.

INTRODUCTION

The Illizi and Berkine basins in southeastern Algeria contain more than 6000 m [19,685 ft] of Paleozoic–Mesozoic strata (Echikh, 1998; Dixon et al., 2010; Galeazzi et al., 2010). The Illizi Basin is separated from the Berkine Basin to the north by the buried axis of the long-lived Ahara high. It is confined by the Amguid-El Biod-Hassi Messaoud ridge to the west, the Tihemboka arch to the east and the Hoggar Massif to the south (Fig. 1). The Illizi Basin is a prolific hydrocarbon province with recoverable reserves estimated at ~5 Bbbl oil and 37 Tcf of gas (Galeazzi et al., 2010). Significant additional resource remains to be discovered based on source rock expulsion estimates (Macgregor, 1998; Cochran and Petersen, 2001).

The Ordovician multi-TCF gas-condensate field in the study area is located in the southern Illizi Basin (Fig. 2), and is a large, low-relief four-way dip closure, approximately 80 km by 50 km [50 mi by 31 mi], with a hydrocarbon column in excess of 100 m [328 ft]**.** The reservoir sequence is comprised of Upper Ordovician (Ashgill) glacial to glacio-marine Unit IV sandstones (Fig. 3). The uppermost Unit IV reservoir contains variable matrix permeabilities ranging from ~0.001 md to ~750 md. The depositional setting of the Upper Ordovician reservoir has been extensively documented in outcrop (e.g., Beuf et al., 1971; Eschard et al., 2005; Ghienne et al., 2007, 2013; Moreau, 2011), and in other offsetting Ordovician fields such as Tin Fouyé Tabankort (Askri et al., 1995; Le Maux et al., 2006), Ohanet (Philippe et al., 2003a), and In Amenas (Dixon et al., 2008; Roussé et al., 2009; Hirst, 2012). The sequence is capped by the lower Silurian Tannezuft-equivalent source rock and seal, which was deposited during eustatic sea-level rise associated with a period of deglaciation (Lüning et al., 2000; Legrand, 2003; Grabowski, 2005; Le Heron and Craig, 2008; Moreau, 2011; Galeazzi et al., 2010).

The burial history of the Illizi Basin is interrogated in this study through integration of regional stratigraphy, sonic compaction analysis, and thermal maturity, fluid inclusion microthermometry, and apatite fission-track data. These data will be used to address: (a) the post-Paleozoic evolution of the basin, (b) the magnitude and timing of maximum burial and temperature within the study area, and (c) the relative timing of hydrocarbon generation and trap formation. It will be demonstrated that trap formation (or at least the current configuration) post-dates the main local hydrocarbon generation events within the basin, and alternative charge mechanisms for the field will be explored.

TECTONIC HISTORY

The Tuareg Shield in North Africa first amalgamated during the Late Neoproterozoic Pan-African orogeny to create the Gondwana supercontinent (e.g., Black et al., 1994; Liégeois et al., 2005). The northern margin of Gondwana was open to the ProtoTethys, creating a vast clastic-dominated Paleozoic sedimentary basin reaching as far south as Niger and Mali (Beuf et al., 1971; Stampfli and Borel, 2002; Guiraud et al., 2005; Konaté et al., 2006; Dixon et al., 2010). During the Pennsylvanian, the Hercynian (Variscan) orogeny caused extensive uplift and erosion along north–south trending arches, resulting in the segmentation of the Saharan Platform into separate basins, such as the Illizi and Mouydir basins (Aliev et al., 1971; Beuf et al., 1971; Fabre, 1976; Boudjema, 1987; Van de Weerd and Ware, 1994; Guiraud et al., 2005). Hercynian erosion penetrated the Cambro-Ordovician sequence on parts of these uplifted highs (e.g., Amguid-El Biod high, Hassi Messaoud ridge, Maouar high; Fig. 2). However, a nearly complete Paleozoic sequence is still preserved in the eastern Illizi Basin (Figs. 2 and 4A), although the original maximum thickness is unknown. Renewed deposition of the Mesozoic–early Cenozoic "Tethys Supersequence" (Boote et al., 1998) occurred in response to subsidence following the initial break-up of Gondwana and the opening of the Tethyan seaway to the north. Triassic fluvial clastics sourced from Hercynian highs were deposited northward in the Berkine Basin (Echikh, 1998). In the northern parts of the Berkine and Oued Mya basins, a Triassic salt basin developed, onlapping to the south toward the Illizi Basin (Turner and Sherif, 2007; Galeazzi et al., 2010; Fig. 4B). Transpressional and strike-slip movements occurred along existing north–south basement lineaments during the Early-Mid Aptian Austrian event, as described along the El Biod trend (Boudjema, 1987; Galeazzi et al., 2010). Sedimentation continued from the Aptian until Mid-Late Eocene inversion (Pyrenean phase), which caused growth of the Atlas Mountains and reactivation of some Austrian and Hercynian fault systems (Echikh, 1998). Intraplate uplift and magmatism also initiated in North Africa during the Mid-Late Eocene, and developed numerous topographic swells, including the Hoggar Massif (e.g., Wilson and Guiraud, 1992; Wilson et al., 1998; Liégeois et al., 2005; Rougier et al., 2013), leading to large-scale exhumation in the flanking sedimentary basins (e.g., English et al., in review A; Fig. 4B).

EVIDENCE FOR A MAJOR INTRA-BASINAL PALEOTOPOGRAPHIC HIGH

The presence of significant post-glaciation paleotopography on the Gondwana shelf during early Silurian time has been demonstrated across many parts of North Africa (e.g., Lüning et al., 2000; Moreau, 2011; Spaak, 2013). In most cases, Silurian shales were deposited directly on Upper Ordovician sandstones during a marine transgression associated with melting of the Late Ordovician ice-caps. Source-rock facies, where present, are typically located at the base of the Silurian shale sequence, and are believed to have generated 80-90% of the Paleozoic-sourced hydrocarbons in North Africa (Boote et al., 1998). The Silurian 'hot' shales are laterally discontinuous and Lüning et al. (2000) proposed that their distribution and thickness were controlled by post-glaciation paleotopography. Spaak (2013) utilized Silurian biostratigraphic data from >300 locations across the Gondwanan shelf to demonstrate that the Silurian onlap is spatially diachronous and reflects progressive infill of the existing topography. While most areas show a duration of Silurian onlap of 5-9 Ma (within the Llandovery), some areas were not flooded until the Ludlow in the late Silurian (Spaak, 2013).

An isopach map of the Silurian shale can be used to identify major paleotopographic features that were present at the end of the Late Ordovician glaciation. For the Illizi and Berkine basins in Algeria, the isopach indicates that the Ordovician field in the study area is located on the southern flank of an early Silurian paleohigh (Fig. 5A). This paleohigh will be herein referred to as the Isarene high. The existence of the Isarene high by early Silurian time can be shown using correlatable shale markers in subsurface wells, which demonstrate that the lower Silurian shale initially infilled lows in the Late Ordovician post-glacial topography. The lowermost Silurian shale within the study area thins toward, and onlaps the paleohigh to the north (Fig. 5B).

In order to confirm diachronous lower Silurian onlap, the graptolitic Silurian shale immediately above the Ordovician reservoir was dated in three wells in the study area (Table 1, Fig. 5C). The oldest Silurian shales were consistently from the *Streptograptus crispus* biozone dated as middle Telychian (Upper Llandovery). In comparison to regional biostratigraphy, the basal Silurian shale has been dated as upper Rhuddanian (Lower Llandovery) (Legrand, 1985, 2003) in outcrops in Tassili N'Ajjer to the south (Fig. 5A), and similar ages have been found from subsurface samples in the Berkine/Ghadames Basin in Algeria and southern Tunisia

(Lüning et al., 2000). These data indicate that the Isarene high was flooded approximately ~5 Ma after the onset of Silurian shale deposition in the Tassili N'Ajjers.

ILLIZI BASIN: TIMING AND MAGNITUDE OF MAXIMUM BURIAL AND PEAK PALEOTEMPERATURES

The burial and thermal history of a basin is important to constrain the hydrocarbon generation history. The timing of peak maturity and maximum burial of the Silurian source rock remains debatable in the southern Illizi Basin due to the removal of a significant part of the stratigraphic record. Some regional studies indicate that the timing of peak maturity was different across the Illizi Basin from Pennsylvanian in the southwest to Late Cretaceous-Eocene in the northeast (Tissot et al., 1984, 1987; Macgregor, 1998; Cochran and Petersen, 2001). In this study, a number of independent methodologies were employed to constrain the timing and magnitude of maximum burial and peak paleotemperatures across the study area.

Sonic Interval Velocity Analysis

Compaction, the reduction of sediment volume during progressive burial, generally results in the reduction of porosity with increasing depth. The degree of compaction of any sediment can be assessed from its sonic velocity, which is a function of lithology, porosity, and fluid in the pore space. This method assumes that porosity is reduced due to mechanical and thermochemical processes, and increasing vertical effective stress (Magara, 1976; Sclater and Christie, 1980; Bulat and Stoker, 1987; Hillis, 1995; Corcoran and Doré, 2005). Extensive work has been done to characterize compaction according to lithology (e.g., Japsen et al., 2007), and shales tend to show a more predictive velocity–depth relationship compared to sandstones (Pryor, 1973; Magara, 1976). Since porosity reduction is largely irreversible, the present-day velocity of correlated shale beds can be used to estimate spatial variations in maximum burial depth.

In order to utilise this method, the compressional sonic velocity for a shale interval is compared to a compaction reference curve, which provides a typical velocity–depth relationship for shale in a normally subsiding basin. A shale is considered overcompacted if its velocity is higher than expected for a given depth, implying the interval was once buried deeper.

Undercompaction can be identified when the measured velocity is lower than expected for that depth. The difference between the present-day depth and the expected depth for the measured velocity equals the amount of apparent exhumation (Corcoran and Doré, 2005; Fig 6A). Previous analyses in the region describe undercompacted sediments in the Berkine Basin and overcompacted sediments in the Illizi Basin (Dixon et al., 2010).

Sonic compaction analyses of 28 wells across a 100 km^2 [39 mi^2] area around the Ordovician field were carried out for the Frasnian and Tournaisian organic-lean shales. Correlatable shale intervals were selected according to spectral gamma-ray curves to avoid organic-rich intervals, which have anomalously low velocities. The Silurian shales were removed from this analysis due to overall lower velocities related to elevated organic content. The average apparent exhumation of each interval was calculated per well using a reference compaction curve derived for sediments with >50% clay content (2 μm size) (*C40* reference curve; Dixon et al., 2010; Fig. 6A). Results indicate that all shale zones are overcompacted compared to their present depth and that the southern part of the field (Well G) is more overcompacted than the northern part (Well A) indicating greater burial depth in the south. An apparent exhumation magnitude grid derived from the wells and reference curve (Fig. 6B) was added to the present-day Top Ordovician depth grid (Fig. 6C) to calculate the maximum burial depth across the field (Fig. 6D). This map illustrates that at maximum burial, the present-day structure was situated on the flank of a much larger paleostructure with its crest located to the north. Using this method, the Top Ordovician is estimated to have reached a maximum depth of ~2.8-2.9 km [9186-9514 ft] in the north (Well A) compared to ~3.1-3.2 km [10,171-10,499 ft] in the south (Well G). Although there is uncertainty associated with the absolute magnitude of apparent exhumation because it depends on the shale reference curve used, the relative compaction differences of 0.2-0.4 km [656-1312 ft] observed across the field are consistent in both shale zones analyzed, and is consistent with a north–south gradient observed in other datasets.

Thermal Maturity

New thermal maturity data from the study area include vitrinite reflectance (R_o%), solid bitumen and chitinozoan reflectance, and Rock-Eval pyrolysis data from 7 wells on the structure (Tables 2 and 3). Solid bitumen reflectance was converted to R_o% equivalent using the relationship from Schoenherr et al. (2007), which is based on a morphology-derived system of

solid bitumen reflectance from Jacob (1989) and Landis and Castano (1995). However, solid bitumen reflectance can be variable (Suárez-Ruiz et al., 2012), and these data were cross-referenced with other thermal indicators (e.g., Rock-Eval pyrolysis, fluid inclusion data) to check for consistency. The chitinozoan reflectance was converted to R_o% equivalent using a relationship from Alpern (1970). Graptolite reflectance data were not available for this study. Rock-Eval pyrolysis data were screened according to published criteria (Peters and Cassa, 1994; English et al., 2015) and converted from T_{max} to R_o% equivalent (Jarvie et al., 2001; Peters et al., 2005).

The results indicate that the thermal maturity of the Ordovician to Carboniferous sequence is elevated in every well compared to what would be predicted due to the deposition of the preserved stratigraphy alone (i.e., the default maturity profile; Fig. 7A). The Silurian source rock in the northern field area has reached the wet gas window (~1.0-1.1 R_o%), whereas the south has reached the wet to dry gas window (~1.2-1.3 R_o%). Measured Ordovician reservoir temperatures from 10 wells across the field indicate an average present-day geothermal gradient of 38°C/km [2.1°F/100 ft] (range 36-41°C/km [2.0-2.2°F/100 ft]) assuming an annual surface temperature of 22°C [72°F] recorded from southern Algerian weather stations. The resulting average modelled present-day basal heat flow is 65 mW/m^2, which is consistent with other estimations of heat flow in the region (60-100 mW/m^2; Lesquer et al., 1990). The maturity data were converted into paleotemperature estimates using *Easy%R_o* (Sweeney and Burnham, 1990) and an assumed heating rate of 1°C/Myr, which is considered to be broadly representative of the Paleozoic phase of burial in the basin. These indicative peak paleotemperatures were then plotted against depth (Fig. 7B). Converted paleotemperature estimates from Wells A, E and H indicate paleogeothermal gradients during maximum burial in the region of 37°C/km [2.0°F/100 ft] (Fig. 7B), which is very similar to the present-day geothermal gradient. In addition to the thermal maturity data, the estimated peak paleogeothermal gradient provides a good fit to modal homogenization temperatures measured in fluid inclusions in Upper Ordovician sandstones, and to the Namurian peak temperature estimates derived from apatite fission-track data (Fig. 7B). The Carboniferous maturity measurements (and associated peak temperature estimates) are slightly elevated compared to the deeper horizons. This may be due to the recycling of older material or due to natural variation in the characteristics of the macerals. In any case, the lower

peak temperature estimates derived from the Carboniferous apatite fission-track data (discussed below) are more in line with paleotemperature trends extrapolated from the deeper horizons.

When the lower Silurian thermal maturity data are superimposed on the sonic compaction-derived Top Ordovician maximum burial map (Fig. 8), both datasets indicate increased maximum burial to the south. Assuming a surface temperature of 24°C [75°F] and a paleogeothermal gradient of 37°C/km [2.0°F/100 ft] during the time of maximum burial (early Eocene), the estimated maximum burial depth of ~2.9 km [9514 ft] for Well A (Fig. 6D) corresponds to a maximum temperature of 131°C [268°F], and the estimated maximum burial depth of ~3.2 km [10,499 ft] for Well G (Fig. 6D) corresponds to a maximum temperature of 142°C [288°F].

Fluid Inclusion Microthermometry

Fluid inclusions are widely used in thermal history, diagenetic and petrographic studies to characterize temperature, salinity and oil gravity of trapped liquid and/or vapour (Roedder, 1984; Walderhaug, 1994; Goldstein, 2001; Blanchet et al., 2003). Fluid inclusion data for 879 inclusions were collected from 39 Ordovician Unit IV core plugs across seven wells in the field. The homogenization temperature (T_h) of each inclusion was optically determined by incrementally heating a polished thin-section containing the inclusion until a vapour bubble dissipated into the inclusion (Walderhaug, 1994; Goldstein and Reynolds, 1994). The salinity of the aqueous inclusions can be estimated by freezing the sample and recording the temperature of the final disappearance of solid during subsequent melting (Bodnar, 1993). The equivalent salinity (wt.%) can then be calculated from the ice-melting temperature (Oakes et al., 1990).

Low-Salinity Aqueous Inclusions

Within the dataset, 88% of inclusions were classified as primary, and 12% as secondary. Both aqueous and oil inclusions were found along quartz grain boundaries and within quartz overgrowths (primary inclusions), and in healed microfractures (secondary inclusions). Based on homogenization temperatures, the earliest primary aqueous inclusions formed at 95°C [203°F], which is typical for the onset of quartz cementation (Lander and Walderhaug, 1999; Walderhaug, 2000). Modal homogenization temperatures from the Upper Ordovician are 135-145°C [275-293°F] in Well A, and higher in Well G at 140-155°C [284-311°F] (Fig. 9). Both are consistent

with thermal maturity measurements and sonic compaction data, which indicate deeper burial in the southern part of the field (Fig. 8). The salinity of the primary inclusions at these modal homogenization temperatures ranges between 4-8 wt.%, and represents most of the dataset (93% in Well A and 71% in Well G). This family of relatively "low" salinity aqueous inclusions records quartz cementation from 95°C [203°F] up to peak temperatures of 135-155°C [275-311°F] (Figs. 9A and 9C) and are interpreted to represent burial phases.

Low-Temperature High-Salinity Aqueous Inclusions

A second group of primary inclusions observed in the wells has dramatically higher salinity (18-25 wt.%), and cooler modal homogenization temperatures of 90-120°C [194-248°F] (Figs. 9B and 9E). A poorly represented intermediate-salinity group (9-16 wt.%) is only 7% of the dataset and may represent a transitional phase between the two main groups (Fig. 9D). The secondary inclusions (12% of entire dataset) (Fig. 9G) are dominantly oil inclusions (83%) co-occurring with high-salinity (>14 wt.%) aqueous inclusions formed at cooler temperatures, (T_h = 103-130°C [217-266°F]), indicating that they are associated with the lower-temperature high-salinity phase. The high-salinity aqueous inclusions are interpreted to post-date the low-salinity aqueous inclusions because: (a) the high-salinity inclusions are not observed to coincide with maximum burial temperatures; (b) healed microfractures containing high-salinity secondary inclusions crosscut both the quartz overgrowths and grain boundaries containing low-salinity inclusions (Fig. 10); (c) the high-salinity aqueous inclusions are closer in composition to the present-day Ordovician formation water (~16 wt.%); and (d) the salinity of primary aqueous inclusions trapped in late-stage barite cement (18-19 wt.%) in Well A yields homogenization temperatures of 98-115°C [208-239°F], which are similar to the present-day reservoir temperature (~95°C [203°F]). The barite cement is interpreted to have precipitated after cooling from maximum burial depth and temperature.

Oil Inclusions

The gravity of oil inclusions ranges from 33-46° API in the wells. In Well A, single-phase oils close to full gas saturation, determined by the similarity of T_h aqueous and T_h oil (Munz, 2001), occur in primary inclusions in quartz overgrowth cements. These single-phase oil inclusions in Well A have an average oil gravity of 37.5° API and are associated with low-

salinity aqueous inclusions with high temperatures (average $T_{h\ Aq}$ = 149°C ± 2°C [300°F ± 4°F] and $T_{h\ Oil}$ = 150°C ± 9°C [301°F ± 16°F]; Fig. 9F). This suggests a minor ~15 m [49 ft] paleo-oil column, restricted to a local ~1 km^2 [0.4 mi^2] paleo-closure, was present at this well location during maximum burial. Secondary oil inclusions in healed microfractures crossing quartz grains and overgrowths are often associated with high-salinity aqueous inclusions with cooler homogenization temperatures (Fig. 9G), and may be related to re-migration of oil during exhumation. Primary petroleum inclusions in the late barite cement in Well A contain phase-separated oil and gas indicating that both were present in the pore system when barite precipitation occurred during or after exhumation. These phase-separated oil inclusions are characterized by an oil gravity of 46° API and homogenization temperatures that are similar to the present-day reservoir conditions (Fig. 9F). This implies that the small paleo-column with 37.5° API oil at maximum temperatures ($T_{h\ Aq\ (Ave)}$ = 149°C ± 2°C [300°F ± 4°F]) was displaced by a two-phase accumulation during barite precipitation ($T_{h\ Aq\ (Ave)}$ = 104°C ± 6°C [219°F ± 10°F]). Since no moveable oil has been encountered in the study area, any minor paleo-oil accumulations are interpreted to have been flushed by gas during or after exhumation. In summary, the fluid inclusion data clearly indicates hotter burial temperatures in the past (modal peak temperatures of 135-155°C [275-311°F] versus present-day reservoir temperatures of ~95°C [203°F]), as well as higher modal temperatures in the southern region compared to the north. These results are consistent with the maximum burial and temperature estimates independently derived from the sonic compaction and other maturity data. The record of single-phase oil inclusions at maximum burial temperatures versus phase-separated oil and gas inclusions at lower temperatures may indicate that phase separation of existing petroleum was an important process during exhumation. Additionally, the significant change in salinity records a notable basinal fluid flow event possibly triggered by exhumation (English et al., in review B).

Apatite Fission-Track Data

Apatite fission-track analysis uses the rate of radioactive decay of uranium and the length and density of damage trails (fission-tracks) in the apatite mineral lattice to constrain the maximum paleotemperature of the grains, and the timing of the last major cooling event (Fleischer et al., 1975; Wagner and Van den Haute, 1992; Green and Duddy, 2012). Apatites were extracted from Well A cuttings ranging in age from Namurian to Ordovician. The complete

dataset and interpretation of different alternative models was discussed by English et al. (in review A), and only the highlights of the preferred thermal history model will be presented here. The measured apatite fission-track ages for all samples are younger than the depositional ages, indicating that the entire preserved stratigraphic sequence was subjected to some degree of fission-track annealing in the past. The default fission-track age profile illustrates the fission-track ages modelled in *HeFTy* (Ehlers et al., 2005) for apatites with 0.1 wt.% chlorine content, assuming no additional burial beyond present-day depths (Fig. 11). This default profile shows a major decrease in fission-track age between present-day temperatures of 60°C [140°F] and 80°C [176°F] due to increased annealing. Total annealing is expected at temperatures above ~100°C [212°F] for apatites of this composition. By comparison, the measured fission-track ages on grains with variable chlorine content are routinely younger than the default profile, which is consistent with the interpretation of hotter temperatures and deeper burial in the past. The Ordovician-Devonian samples are interpreted to have been totally annealed in the past and all apatite grains are dominated by Eocene and younger fission-track ages (English et al., in review A). The shallower Carboniferous samples reached lower peak temperatures and have only been partially annealed in the past. The actual fission-track ages for the shallower samples bear no relation to any specific cooling event; the fission-track age itself only dates a cooling event if the samples cooled rapidly through the partial annealing zone. Inverse modelling of the fission-track ages and track length data for the Namurian sample using *HeFTy* provided a best-fit model with the onset of cooling from peak temperature during the Eocene (English et al., in review A). The results of the inverse modelling suggest that the most likely Cenozoic peak temperature for the Namurian sample was in the 60-75°C [140-167°F] range (i.e., 30-45°C [54-81°F] hotter than present-day temperatures). Marginally higher peak temperatures (+5-10°C [9-18°F]) are allowed by the Namurian fission-track data if maximum temperature occurred during the Jurassic or Cretaceous (English et al., in review A), and was followed by a significant cooling event, but there is no strong geological evidence to support a major Mesozoic exhumation event at this locality (e.g., see cross-sections across Tin Fouyé Tabankort in Chiarelli, 1978; Boote, 2013). In Well A, the best-fit thermal history model for the Namurian sample allows for the Top Ordovician reservoir temperature to reach 140°C [284°F] at maximum burial prior to Cenozoic cooling to ~95°C [203°F] present-day (English et al., in review A). Therefore, the apatite fission-

track dataset provides independent support for estimates of maximum burial depth and temperature based on the sonic compaction, thermal maturity and fluid inclusion studies, and additionally provides constraints on the timing of the last major exhumation event.

RECONSTRUCTING MISSING STRATIGRAPHY

As petroleum systems modelling of a sedimentary basin requires the complete depositional and erosional history, it is necessary to fill in any gaps in the preserved stratigraphic record. The rationale behind the assumptions of missing stratigraphy are discussed below.

Eroded Paleozoic (Pre-Hercynian) Stratigraphy

The Hercynian subcrop pattern, beneath younger Mesozoic cover, is well documented across the Illizi-Berkine region (Galeazzi et al., 2010), showing a broadly W-E erosional gradient dominated by the unroofing of the Amguid–El Biod–Hassi Messaoud ridge to the west (Figs. 2 and 4A). In contrast, the Cenozoic exhumation was dominated by uplift of the Hoggar Massif to the south, superimposing a later N-S erosional gradient across the Illizi Basin (Galeazzi et al., 2010; English et al., in review A; Figs. 2 and 4B). The maximum preserved Carboniferous section in the eastern Illizi Basin is ~1.3-1.4 km [4265-4593 ft] thick (Chaouchi et al., 1998; Galeazzi et al., 2010), providing a minimum pre-erosion estimate of Carboniferous thickness. The preserved Carboniferous in Well A is ~890 m [2920 ft] thick with Westphalian-Namurian strata at the surface, while the younger Westphalian to Stephanian section is now absent. Paleozoic sedimentation may have continued into the Early Permian as indicated by lagoonal sediments of Stephanian-Autunian age that are described in the Oued Mya Basin (Lefranc and Guiraud, 1990). Hercynian exhumation is assumed to have begun at 286 Ma in the Permian in this study (Yahi et al., 2001).

One uncertainty with respect to the burial history reconstruction is how much of the missing Carboniferous and Permian section was eroded during the Hercynian event and how much was eroded during later Cenozoic exhumation. The Hercynian unconformity crops out approximately 17 km [10.6 mi] to the north of Well A (Fig. 2) and dips an average of ~0.4-0.8 degrees in a northerly direction into the central Illizi Basin region (Fig. 4B). When the Hercynian unconformity is projected southward over the Well A location, the thickness below this plane

suggests that ~200-300 m [656-984 ft] of Carboniferous stratigraphy was preserved after Hercynian exhumation, but eroded later in the Cenozoic. The preserved and eroded thicknesses of the Paleozoic strata increase southward to Well G, which was deeper off the flank of the Paleozoic paleohigh. Total estimated missing Carboniferous and Permian stratigraphy for Well A and Well G is summarized in Table 4 based on regional data and model iterations to achieve the best-fit of the data.

Eroded Mesozoic and Cenozoic (Post-Hercynian) Stratigraphy

The Mesozoic and Cenozoic depositional history of the study area was reconstructed using well data, surface geology maps (Yarmolyuk and Kuznetsov, 1977; Choubert and Faure-Muret, 1990) and publications (Lefranc and Guiraud, 1990; Yahi et al., 2001; Rossi et al., 2002; Dixon et al., 2010; Galeazzi et al., 2010; Boote, 2013; Table 4). Following the Hercynian event, a Triassic salt basin formed in the northern portion of the Berkine and Oued Mya basins during Triassic-Liassic extension, followed by progressive shoreline migration southward during the Late Mesozoic (e.g., Galeazzi et al., 2010). Triassic continental deposits in the Berkine Basin originated from Hercynian uplifts, such as the El Biod and Dahar highs (Echikh, 1998; Figs. 2 and 5). The southern pinch-out of Triassic sandstone is 120-190 km [75-118 mi] north of the study area (between 29°-30° latitude, Galeazzi et al., 2010; Fig. 4B), while Triassic-Jurassic fluvial-lacustrine deposits also crop out 40-50 km [25-31 mi] east of Well A (Choubert and Faure-Muret, 1990), showing progressive onlap westward toward the study area (English et al., in review A). Based on these observations, post-Hercynian deposition is assumed to have resumed in the study area during the Middle Jurassic (see Fig. 4B), and the Triassic to Lower Jurassic is interpreted to be a period of non-deposition or bypass.

Following inundation during the Middle Jurassic, the study area is assumed to have been a site of extensive Mesozoic–early Cenozoic deposition interrupted only by the relatively minor Austrian tectonic event (Galeazzi et al., 2010). The magnitude and timing of additional burial was calibrated to stratigraphic observations in the Berkine Basin and to thermal maturity and apatite fission-track data. Previous interpretations have considered that the Hoggar Massif, south of the Illizi Basin, remained an exposed topographic high from the time of the Hercynian orogeny until present-day (Fabre, 1976; Guiraud et al., 2005; Liégeois et al., 2005). However, remnants of Jurassic to Cretaceous sediments are widely preserved on the flanks of the uplifted

Hoggar Massif (Bordet, 1954; LeFranc and Guiraud, 1990; Busson et al., 1999; Philippe et al., 2003b) and recent thermochronometric data from the Hoggar (Rougier et al., 2013) suggest that Cretaceous to Paleocene strata may have covered a large part of this region prior to Eocene uplift and exhumation (English et al., in review A).

Middle to Late Mesozoic subsidence in the North African platform was punctuated by transpressional deformation along pre-existing north–south trending structures, such as the Amguid-El Biod trend (Galeazzi et al., 2010; Figs. 1 and 2), during the Late Neocomian-Middle Aptian Austrian event (Fig. 3). The significance of this event within more internal parts of the Illizi Basin is less defined and only a relatively minor associated unconformity is observed at Tin Fouyé Tabankort (Chiarelli, 1978; Boote, 2013), 70 km [43 mi] north-northwest of the study area (Fig. 1). A minor amount of Mid-Aptian (Austrian) exhumation is included in the burial history models to account for this unconformity (Table 4). Based on the apatite fission-track data from Well A, and extensive regional thermochronometric data, maximum burial in the study area is interpreted to have occurred during the early Eocene before major exhumation associated with uplift of the Hoggar Massif (English et al., in review A).

INTEGRATED 1D BURIAL HISTORY MODELS

Well-based 1D (one-dimensional) burial history modelling was carried out using *Genesis* (Zetaware) to constrain the thermal history of the field and the timing of hydrocarbon generation from the overlying lower Silurian source rock. Wells A and G were selected as representative of the northern and southern parts of the field. The wells were divided into 58 stratigraphic and erosional events (Table 4). As outlined in the previous section, regional stratigraphic observations were incorporated to help reconstruct the eroded stratigraphy, and the 1D models were calibrated to available thermal maturity and apatite fission-track data.

Boundary Conditions

Paleosurface temperatures were derived from paleolatitude reconstructions (Wygrala, 1989; Underdown, 2006) and paleobathymetric inputs were modified from previous Berkine Basin studies (Yahi et al., 2001) to delay the onset of flooding in the study area until the Middle Jurassic. Heat flow from base of the sediment column was specified in the model, and the

geothermal gradient varied through time according to lithology, conductivity and burial rate. The petrophysical properties for each of the different lithologies are listed in Table 5. As discussed in the thermal maturity section, an average present-day basal heat flow (65 mW/m^2) was calculated for the field based on modern temperature data from the wells. This basal heat flow was held constant through time in the 1D models due to: (a) lack of evidence for a major rifting event in the region (Fig. 4), and (b) similar magnitudes of the present-day geothermal gradient and the estimated paleogeothermal gradient during maximum burial (Fig. 7B). Although it is unlikely that basal heat flow remained constant throughout this time, none of the datasets used for calibration required a variable heat flow model.

Simulation Results

The 1D modelling indicates that elevated peak temperatures compared to present-day are required to achieve a best-fit for all the datasets. In Well A, maximum paleotemperature was modelled at ~140°C [284°F] for the Upper Ordovician reservoir and the basal Silurian source rock with a maximum burial depth of 2.95 km [9678 ft] during the early Eocene (Fig. 12A). This thermal history model provided a reasonable fit to available apatite fission-track for Well A (Fig. 11), as well as good agreement with the maximum paleotemperatures estimated from the thermal maturity and fluid inclusion data.

The Well G model in the southern part of the field requires deeper burial (~3.37 km [11,056 ft]), hotter maximum paleotemperatures (~156°C [313°F]), and more Cenozoic exhumation compared to the Well A model (Fig. 12B). The main differences between the northern Well A and the southern Well G burial history models are as follows:

- The sonic compaction analysis indicates that Well G was buried ~400 m [1312 ft] deeper than Well A. About 215 m [705 ft] of this additional burial can be ascribed to southward thickening of the preserved stratigraphic section (43 m [141 ft], 85 m [279 ft], and 86 m [282 ft] in the Silurian, Devonian and Carboniferous, respectively). The eroded Carboniferous stratigraphy is assumed to thicken from Well A to Well G in the same proportion as the preserved Carboniferous section.

- Hercynian erosion was estimated to be 50 m [164 ft] less in Well G compared to Well A (Table 4) based on the Hercynian subcrop pattern, which indicates increasing Hercynian exhumation in a north-westward direction (Fig. 2).
- An additional ~100 m [328 ft] of post-Hercynian strata was input at Well G to achieve a better fit to the thermal maturity data and hotter modal fluid inclusion temperatures. This additional section was assigned to the Lower Cretaceous because the Neocomian-Albian section is observed to thicken toward the west of the basin (Fig. 4A).
- The magnitude of Cenozoic exhumation is higher in Well G (~1.4 km [4593 ft]) than Well A (~1.0 km [3281 ft]). This is consistent with the regional interpretation of increasing Cenozoic exhumation southwards toward the Hoggar Massif (Figs. 2 and 4B; English et al., in review A).

The final models result in ~16°C [29°F] difference in maximum paleotemperature between the north (Well A) and south (Well G) (Fig. 13) at 140°C [284°F] and 156°C [313°F] respectively. It is noteworthy that the maximum pre-Hercynian paleotemperatures reached in the Carboniferous (Well A = 137°C [279°F]; Well G = 145°C [293°F]) are very close to the maximum paleotemperatures modelled in the early Eocene. While the apatite fission-track data for Well A require the onset of significant cooling in the Eocene, maximum paleotemperatures may have occurred during the Carboniferous-Permian in other parts of the Illizi Basin where thicker Paleozoic and thinner Mesozoic sections were deposited (e.g., Tissot et al., 1987).

Timing of Hydrocarbon Generation and Expulsion

In the Illizi Basin, the basal Silurian source rock is characterized by oil-prone marine Type II kerogen (e.g., Cole et al., 2000) with a present-day TOC (total organic carbon) content ranging from 2-14 wt.% (Table 3). As these samples had reached the late oil to early gas window, the original TOC content for the source rock must have been much higher. Source rock kinetic parameters have been measured on immature Silurian samples from the Berkine Basin in Algeria (Makhous et al., 1997). The mean activation energy reported by Makhous et al. (1997) is typical of other Type II marine source rocks (organofacies B, Pepper and Corvi, 1995; Devonian-Mississippian Woodford shale, Arbuckle Mountains, Oklahoma, Lewan and Ruble, 2002). Source rock modelling was carried out using *Kinex v.4.7* and *Genesis v. 5.5*, using parameters

listed in Table 6. Hydrocarbon generation and expulsion from the Silurian source rock began during the Carboniferous (Fig. 14). Just prior to the Hercynian exhumation event, the Silurian source rock reached paleotemperatures of ~137°C [279°F] and ~145°C [293°F] in Well A and Well G, with respective transformation ratios of ~80% and ~87%. These models indicate that a significant proportion of the generative potential of the Silurian source rock was expelled prior to the Hercynian event, although lower basal heat flow assumptions during the Paleozoic would result in greater retention of the source rock generative potential. The hydrocarbon generation system was subsequently switched off due to Hercynian exhumation and cooling. Post-Hercynian reburial reinitiated hydrocarbon generation and expulsion during the Cretaceous and Paleocene before the last major exhumation event initiated in the Eocene (Fig. 14). The present-day transformation ratio of the Silurian source rock is estimated around 90% at Well A and 95% at Well G. These modelled transformation ratios are consistent with estimates of ~90-93% interpreted from available Rock-Eval pyrolysis data on lower Silurian core samples (Table 3; formula from Jarvie et al., 2007).

DISCUSSION

Relative Timing of Trap Formation and Petroleum Charge

The Ordovician field in the study area is located on the southern flank of a long-lived regional Paleozoic high, herein termed the Isarene high. This paleohigh was present at the end of the Late Ordovician glaciation as evidenced by basal Silurian onlap patterns (Fig. 5B), and the gross Silurian isopach (Fig. 5A). Sonic overcompaction maps (Fig. 6) and thermal maturity data (Fig. 8) both indicate that this regional paleohigh persisted in the subsurface with a similar geometry until maximum burial in the early Eocene. Some minor eastward tilting may have occurred during the Hercynian event (Fig. 2). Major basin-scale exhumation during the Middle Cretaceous Austrian event is discounted for reasons stated previously, although Austrian deformation is locally significant on major pre-existing structures – particularly along the western basin margin (i.e., Amguid-El Biod trend). It is noteworthy that local small-scale structural closures superimposed on the regional paleohigh may have been charged with oil prior to maximum burial (e.g., single-phase oil inclusions in Well A). The major northward tilting of

the Illizi Basin in response to the uplift of the Hoggar Massif to the south resulted in the reconfiguration of the structural nose (Fig. 6D), creating the four-way dip closure observed present-day (Fig. 6C).

Independent assessment of the timing of trap formation can be established by reversing the average northward Eocene tilt of 0.6° in this area to reconstruct the maximum burial geometry. Applying this tilt to the present-day Top Ordovician structure map results in a structural geometry that is very similar to the maximum burial map derived from the sonic overcompaction study (Fig. 15). This observation provides confidence that the study area was located on the southern flank of a regional paleostructure that persisted from the Paleozoic (Fig. 5) to early Eocene time (Fig. 15), and that the broad low-relief four-way structural closure that defines the present-day petroleum trap formed during Eocene-Miocene uplift and exhumation of the Illizi Basin. As most of the hydrocarbon generation and expulsion at this location occurred in the Carboniferous and Cretaceous-Paleocene (Fig. 14), it is also clear that the timing of trap formation post-dates the primary hydrocarbon generation events in the Illizi Basin (Fig. 16).

Possible Charge Mechanisms for the Ordovician Field

Conventional wisdom dictates that hydrocarbon charge effectively shuts off once the source rocks have been uplifted and cooled from their peak burial depths and temperatures. Although low-level kinetic generation may continue during the initial cooling phase, the magnitude of Eocene exhumation and cooling in the Illizi Basin resulted in a cessation of petroleum generation in the study area (Fig. 14). Therefore, alternative models are required to explain the post-exhumation gas-condensate charge of this Ordovician field. Doré et al. (2002) reviewed charge processes associated with exhumed sedimentary basins, and concluded that post-exhumation charging of traps can only occur via the redistribution of hydrocarbons already existing within the basin, unless the exhumed basin is on a long-distance hydrocarbon migration route from an adjacent continuously subsiding basin. Four different charging mechanisms for exhumed basins are discussed here: (1) long-distance migration from an adjacent unexhumed basin; (2) tertiary migration; (3) phase separation and gas expansion; and (4) exhumation charge.

Any or all of these mechanisms may have contributed to charging the Ordovician field in the study area.

Long-Distance Migration from an Adjacent Unexhumed Basin

The Illizi Basin is separated from the Berkine Basin to the north by the buried axis of the long-lived Ahara high (Galeazzi et al., 2010). While Cenozoic exhumation occurred across the Illizi Basin, the magnitude of this exhumation event decreases northward into the Berkine Basin, and is minimal in the main depocenter where a largely complete Mesozoic-Cenozoic section is preserved (Fig. 4B). Previous basin modelling studies of the Berkine Basin (Yahi et al., 2001; Underdown and Redfern, 2008) indicate that the lower Silurian source rock in the central Berkine Basin reached maximum generative potential during pre-Hercynian burial (TR = 0.9-1.0), and is largely overmature today. Hence, present-day, long-distance, southward migration from the unexhumed central portion of the Berkine Basin is not a likely mechanism for charging post-exhumation traps in the Illizi Basin.

However, Daniels and Emme (1995) observed that the thermal maturity of the lower Silurian shale decreases toward the flanks of the Berkine Basin, and over the Ahara high itself (from <1.1 to 1.3 R_o%), and this is likely due to pronounced thinning of the Paleozoic section over this region (Fig. 4B). This level of peak thermal maturity broadly equates to the onset of wet gas generation (Daniels and Emme, 1995), similar to the observed maturity within the study area (Fig. 8), and, therefore, this region around the Ahara high is a potential candidate for actively charging the Ordovician gas-condensate fields in the Illizi Basin further south. The hydrocarbon generation model from this study (Fig. 14) indicates that Cenozoic exhumation effectively shut-off active generation and expulsion within the Illizi Basin itself. This is also probably the case on the southern flank of the Ahara high where Turonian and older strata crop out at the surface. However, the magnitude of exhumation is expected to decrease toward the northern flank of the Ahara high, on the southern margin of the Berkine Basin (Fig. 4B). Up to 600 m [1969 ft] of Senonian strata were deposited in the central Berkine Basin (Yahi et al., 2001; Rossi et al., 2002), while only ~150 m [492 ft] of basal Senonian strata are preserved on the northern part of the Ahara high. Although the full Senonian sequence of the Berkine Basin may have originally thinned southward onto the Ahara high, it does suggest the potential for up to 450 m [1476 ft] of exhumation on the northern flank of the Ahara high. Sensitivity analysis on Well

A indicates that approximately 300 m [984 ft] of exhumation or greater is sufficient to significantly reduce subsequent gas and oil generation and expulsion (Fig. 17). However, since modelling has not been conducted on this region specifically, we cannot rule out the possibility that there is a narrow band along the northern flank of the Ahara high, on the southern margin of the Berkine Basin, where wet gas generation and expulsion may be occurring, and potentially contributing, via southward long-distance migration, to the recent charging of the Ordovician gas-condensate fields in the Illizi Basin. A regional 3D basin model would be required to more rigourously test this hypothesis.

Tertiary Migration

Tertiary migration (remigration) of petroleum fluids within sedimentary basins may occur during exhumation due to basin tilting, trap modification, seal failure, or reconfiguration of hydrodynamic gradients. The fluid inclusion data from the Ordovician sandstone in the field area records the presence of low-salinity formation water at maximum burial conditions, followed by high-salinity formation water at lower temperatures (Fig. 9). We interpret that these high-salinity fluids migrated into the field area during or after Eocene exhumation as they are not associated with maximum paleotemperatures, and are the closest match to the present-day formation water salinities in the field.

The present-day formation water in the field is characterized as $CaCl_2$ formation water with low SO_4 and HCO_3, and low Cl/Br and Na/Br ratios (English et al., in review B). This type of water is often associated with the progressive evaporation of seawater beyond the point of halite precipitation (Rittenhouse, 1967; Carpenter, 1978; Walter et al., 1990; Hanor, 1994; Kesler et al., 1995). Therefore, one possible origin for these high-salinity formation waters is the Triassic-Lower Jurassic evaporitic sequences found present-day in the Berkine Basin (Chiarelli, 1978; Turner and Sherif, 2007; English et al., in review B). In regions where the Hercynian unconformity cuts deeply into the Paleozoic, such as the Hassi Messaoud ridge (Fig. 2), Mesozoic rocks were deposited directly on the Cambro-Ordovician sequence (e.g., Zeroug et al., 2007; Galeazzi et al., 2010). Hence, the residual high-salinity brines from Mesozoic evaporitic formations may have infiltrated the Ordovician section via subcrop juxtaposition along the Hercynian unconformity at these locations (English et al., in review B) as a result of density-

driven brine reflux that can penetrate deeply into a sedimentary column (e.g., Bein and Dutton, 1993; Ceriani et al., 2002).

The flux of formation waters over long distances into the Illizi Basin during, or after, Eocene exhumation suggests that long-distance remigration of pre-existing hydrocarbons within the Illizi and Berkine basins may also have occurred at this time. The low-temperature high-salinity (>18 wt.%) inclusions are found only in primary barite and quartz cements (Figs. 9B and 9E) in permeable sandstones (> 1 md), suggesting that formation water was mobile in the matrix pore system during this basin-wide flux. Additionally, low-temperature high-salinity secondary inclusions associated with oil inclusions (Fig. 9G) are dominantly found in healed microfractures in the lower-permeability sandstones and also provide evidence of hydrocarbon remigration during exhumation. This observation suggests that late-stage microfracturing, possibly linked to thermal contraction during cooling (English, 2012), may be important for providing permeable pathways in the tighter formations.

Phase Separation and Gas Expansion

Petroleum is likely to exist as a single phase at pressures and temperatures in excess of 28 MPa [4061 psi] and 95°C [203°F], respectively (Katz, 1959). This is likely to have been the case at Well A, where single-phase oil inclusions, close to full gas saturation, are found in primary quartz overgrowth cements (Fig. 9F). We interpret that these primary oil inclusions record the presence of a minor ~15 m [49 ft] paleo-oil column close to maximum paleotemperatures at this location (T_h = 147-151°C [297-304°F] in oil, and oil-associated aqueous inclusions). If the liquid phase is fully saturated with respect to gas (i.e., at bubble-point) at maximum burial, the oil will volumetrically shrink during exhumation as gas exsolves from the liquid phase (see discussion in English et al., 2016). Late-stage primary inclusions in barite cement in Well A, with phase-separated oil and gas trapped at 98-115°C [208-239°F] (Figs. 9B and 9F), may provide evidence of this process in the study area. The expansion of the separated gaseous phase will lead to a net increase in hydrocarbon volume under the new pressure-temperature conditions, and gas may displace oil from existing traps and lead to remigration or hydrocarbon losses from the system. Any newly formed traps in an up-dip position in the basin may be charged during this late-stage flux of hydrocarbons. Additionally, methane exsolution from formation water may also lead to significant gas volumes being released during exhumation (Doré et al, 2002), particularly in this

case, as methane solubility in the formation water is reduced due to decreased temperature and increased salinity.

Exhumation Charge

During exhumation, volumetric expansion of the gaseous phase drives incremental volumes of petroleum out of the source rock, as the interstitial pore pressure in the source rock re-equilibrates to the new post-exhumation pressure conditions (English et al., 2016). English et al. (2016) calculated that, for a gas-saturated source rock, the incremental volume of free gas migrated per 1 km^2 [0.4 mi^2] area, 1 m [3.3 ft] source rock thickness and 1% gas-filled porosity is 0.01 MMcm [0.35 MMcf] for each incremental unit decrease in the gas expansion factor (GEF) during exhumation. To estimate charge volumes for a gas case, we can assume an average lower Silurian source rock thickness of 10 m [33 ft] with 4% gas-filled porosity and that major exhumation occurred over an area of 75,000 km^2 [28,958 mi^2] in the Illizi Basin. Using the burial history model from this study as a guide, we can assume a peak pressure of 46 MPa [6672 psi] (14 kPa/m [0.62 psi/ft] overpressure at 3.3 km [10,827 ft] peak burial depth due to active petroleum generation) and a peak temperature of 160°C [320°F]. Typical present-day conditions can be taken as 19 MPa [2756 psi] pressure and a temperature of 90°C [194°F]. Taking a gas gravity of 0.7, we have a reduction in GEF from 265 at peak burial to 175 after exhumation. Using these inputs, we predict that the matrix pore system of the lower Silurian source rock should release 2.7 Tcm [95 Tcf] of gas due to pressure equilibration during and after the exhumation event. These incremental 'exhumation charge' volumes are likely to be mostly released into the underlying Ordovician or fault juxtaposed reservoirs. Traps in an up-dip position in the basin could be charged via this mechanism.

CONCLUSIONS

Analysis of the burial and thermal history of an Ordovician field in the Illizi Basin using new thermal maturity, apatite fission-track, fluid inclusion microthermometry, sonic velocity and biostratigraphic data provides independent, and consistent constraints on the temporal evolution of the structure. The following conclusions have been drawn:

(1) The preserved Paleozoic sequence in the study area experienced elevated temperatures in the past, initially due to burial prior to Hercynian exhumation and again during reburial in the Mesozoic and early Cenozoic.

(2) The available data indicates that maximum burial most likely occurred in the early Eocene with estimated maximum burial depths for the top Ordovician ranging from 2.95 km [9678 ft] in the northern part of the field (Well A) to 3.37 km [11,056 ft] in the southern part of the field (Well G). The corresponding estimates of maximum paleotemperature are 140°C [284°F] and 156°C [313°F] respectively.

(3) The field is located on the southern flank of a long-lived regional paleotopographic high, which was present at least by early Silurian time. This paleostructure persisted in the subsurface throughout the Paleozoic and Mesozoic. Maximum burial occurred during the early Eocene, prior to uplift of the Hoggar Massif and northwards tilting of the Illizi Basin.

(4) The Cenozoic exhumation event resulted in northward tilting of the paleostructural nose and the formation of the large present-day structural trap in the study area. The magnitude of exhumation increases southward with ~1.0 km [3281 ft] of exhumation in the north of the field (Well A) and ~1.4 km [4593 ft] in the south (Well G).

(5) The lower Silurian source rocks initially began to generate oil in the Carboniferous, switching off during Hercynian exhumation before resuming generation in the Mesozoic following renewed subsidence. The lower Silurian source rock entered the gas window during the Late Cretaceous–early Eocene.

(6) Trap formation in the study area post-dates the primary hydrocarbon generation events in the burial history models. The present-day gas-condensate accumulation is proposed to have been charged by one or a combination of: (a) long-distance migration from an area of active hydrocarbon generation on the southern margin of the Berkine Basin; (b) remigration of existing gas within the basin - possibly associated with the late-stage migration high-salinity formation waters; (c) phase-separation and gas expansion within exhumed pre-existing oil and gas accumulations, as supported by the presence of phase-separated oil and associated gas in late-stage petroleum inclusions; and/or (d) late-stage

charge during the depressuring of the overlying source rocks during or after the exhumation event as demonstrated by modelling work in English et al. (2016).

(7) Although play types where trap formation post-dates the main hydrocarbon generation and expulsion phase are typically downgraded in petroleum system risk analysis, this work supports a model in which up-dip traps on the flanks of exhumed petroliferous basins may be charged via re-distribution of pre-existing hydrocarbons within the basin.

REFERENCES CITED

Aliev, M., N. Aït Laoussine, V. Avrov, G. Aleksine, G. Barouline, B. Lakovlev, M. Korj, J. Kouvykine, V. Makarov, V. Mazanov, E. Medvedev, O. Mkrtchiane, R. Moustafinov, L. Oriev, D. Oroudjeva, M. Oulmi, and A. Saïd, 1971, Geological structures and estimation of oil and gas in the Sahara in Algeria: Spain, Altamira-Rotopress, S.A., 265 p.

Alpern, B., 1970, Classification petrographie des constituents organiques fossiles des roches sedimentaires: Revue de l'Institut Francais du Petrole, v. 25, p. 1233-1267.

Askri, H., A. Belmecheri, B. Benrabah, A. Boudjema, K. Boumendjel, M. Daoudi, M. Drid, T. Ghalem, A.M. Docca, H. Ghandriche, A. Ghomari, N. Guellati, M. Khennous, R. Lounici, H. Naili, D. Takherist, and M. Terkmani, 1995, Géologie de l'Algérie (Geology of Algeria): Bath, UK, Schlumberger-Sonatrach Well Evaluation Conference 1995, 93 p.

Bein, A., and A.R. Dutton, 1993, Origin, distribution, and movement of brine in the Permian Basin (U.S.A.): A model for displacement of connate brine: GSA Bulletin, v. 105, p. 695–707, doi: 10.1130/0016-7606(1993)105<0695:ODAMOB>2.3.CO;2.

Beuf, S., B. Biju-Duval, O. de Charpal, P. Rognon, O. Gariel, and A. Bennacef, 1971, Les grès du Paléozoïque inférieur au Sahara: Paris, Publications de l'Institut Français du Pétrole, Coll. Science et Technique du Pétrole 18, 464 p.

Black, R., L. Latouche, J.P. Liégeois, R. Caby, and J.M. Bertrand, 1994, Pan-African displaced terranes in the Tuareg Shield (central Sahara): Geology, v. 22, p. 641-644, doi: 10.1130/0091-7613(1994)022<0641:PADTIT>2.3.CO;2.

Blanchet, A., M. Pagel, F. Walgenwitz, and A. Lopez, 2003, Microspectrofluorometric and microthermometric evidence for variability in hydrocarbon fluid inclusions in quartz overgrowths: implications for inclusion trapping in the Alwyn North field, North Sea. Organic Geochemistry, v. 34, p. 1477-1490, doi: 10.1016/j.orggeochem.2003.08.003.

Bodnar, R.J., 1993, Revised equation and table for determining the freezing point depression of H_2O-NaCl solutions: Geochimica et Cosmochimica Acta, v. 57. p. 683-684, doi: 10.1016/0016-7037(93)90378-A.

Boote, D., 2013, The 'Austrian Event' of the Afro-Arabian Plate and its influence upon Cretaceous petroleum systems: AAPG Search and Discovery Article #90161, 2003 AAPG European Regional Conference, Barcelona.

Boote, D.R.D., D.D. Clark-Lowes, and M.W. Traut, 1998, Palaeozoic petroleum systems of North Africa, *in* D.S. MacGregor, R.T.J. Moody, and D.D. Clark-Lowes, eds., Petroleum geology of North Africa: Geological Society, London, Special Publication 132, p. 7-68, doi: 10.1144/GSL.SP.1998.132.01.02.

Bordet, P., 1954, La série de Serouenout (Ahaggar oriental) est d'âge "Continental Intercalaire" (Crétacé Moyen): Comptes Rendus de l'Académie des Sciences, v. 238, p. 500-503.

Boudjema, A., 1987, Evolution structural du basin petrolier Triasique du Sahara Nord Oriental (Algérie): Ph.D. thesis, Université de Paris-Sud, Centre d'Orsay, 290 p.

Bulat, J., and S.J. Stoker, 1987, Uplift determination from interval velocity studies, UK Southern North Sea, *in* J. Brooks, and K. Glennie, eds., Petroleum Geology of North West Europe: London, Graham and Trotman, p. 293-305.

Busson, G., A. Dhondt, F. Amédro, D. Néraudeau, and A. Cornée, 1999, La grande transgression du Cénomanien supérieur-Turonien inférieur sur la Hamada de Tinrhert (Sahara algérien): Datations biostratigraphiques, environnement de dépôt et comparaison d'un témoin épicratonique avec les séries contemporaines à matière organique du Maghreb: Cretaceous Research, v. 20, p. 29-46, doi: 10.1006/cres.1998.0137.

Carpenter, A.B., 1978, Origin and chemical evolution of brines in sedimentary basins: Society of Petroleum Engineers, SPE-7504-MS, doi: 10.2118/7504-MS.

Ceriani, A., A. Di Giulio, R.H. Goldstein, and C. Rossi, 2002, Diagenesis associated with cooling during burial: An example from Lower Cretaceous reservoir sandstones (Sirt Basin, Libya): AAPG Bulletin, v. 86, p. 1573-1591, doi: 10.1306/61EEDD0A-173E-11D7-8645000102C1865D.

Chaouchi, R., M.S. Malla, and F. Kechou, 1998, Sedimentological evolution of the Givetian-Eifelian (F3) sand bar of the West Alrar field, Illizi basin, Algeria, *in* D.S. MacGregor, R.T.J. Moody, and D.D. Clark-Lowes, eds., Petroleum geology of North Africa:

Geological Society, London, Special Publication 132, p. 187-200, doi: 10.1144/GSL.SP.1998.132.01.11.

Chiarelli, A., 1978, Hydrodynamic framework of eastern Algerian Sahara – Influence on hydrocarbon occurrence: AAPG Bulletin, v. 62, p. 667-685.

Choubert, A., and A. Faure-Muret, 1990, International geological map of Africa: CGMW (Commission of the Geological Map of the World), UNESCO, Paris, France, scale 1:5,000,000, 6 sheets.

Cochran, M.D., and L.E. Petersen, 2001, Hydrocarbon exploration in the Berkine Basin, Grand Erg Oriental, Algeria, *in* M.W. Downey, J.C. Threet, and W.A. Morgan, eds., Petroleum provinces of the twenty-first century: Tulsa, AAPG Memoir 74, p. 531-557.

Cole, G., Z.A. Yu, M. Arab, D. Kassab, P. Cutts, T. Pimble, and M. Jones, 2000, Petroleum geochemistry and 2-D modelling of the Boukhechba permit, Illizi Basin, Algeria: 4th Middle East Geosciences Conference, GEO 2000, v. 5, p. 68-69.

Corcoran, D.V., and A.G. Doré, 2005, A review of techniques for the estimation of magnitude and timing of exhumation in offshore basins: Earth Science Reviews, v. 72, p. 129-168, doi: 10.1016/j.earscirev.2005.05.003.

Daniels, R.P., and J.J. Emme, 1995, Petroleum system model, eastern Algeria from source rock to accumulation: When, where and how?: Proceedings of the seminar on source rocks and hydrocarbon habitat in Tunisia, Entreprise Tunisienne d'Activitiés Pétrolières (ETAP) Memoir 9, p. 101-124.

Dixon, R.J., T.L. Patton, J.P.P. Hirst, and J. Diggens, 2008, Transition from subglacial to proglacial depositional systems: Implications for reservoir architecture, Illizi Basin, Algeria: AAPG Search and Discovery, article 50095, http://www.searchanddiscovery.com/documents/2008/08180dixon/dixon-50095.pdf (accessed December 10th, 2014).

Dixon, R.J., J.K.S. Moore, M. Bourne, E. Dunn, D.B. Haig, J. Hossack, N. Roberts, T. Parsons, and C.J. Simmons, 2010, Integrated petroleum systems and play fairway analysis in a

complex Palaeozoic basin: Ghadames-Illizi Basin, North Africa: Geological Society, London, Petroleum Geology Conference series 7, p. 735-760, doi: 10.1144/0070735.

Doré, A.G., D.V. Corcoran, and I.C. Scotchman, Prediction of the hydrocarbon system in exhumed basins, and application to the NW European margin, *in* A.G. Doré, J.A. Cartwright, M.S. Stoker, J.P. Turner, and N. White, 2002, Exhumation of the North Atlantic Margin: Timing, Magnitude and Implications for Petroleum Exploration: Geological Society, London, Special Publications 196, p. 401-429, doi: 10.1144/GSL.SP.2002.196.01.21.

Echikh, K., 1998, Geology and hydrocarbon occurrences in the Ghadames Basin, Algeria, Tunisia, Libya, *in* D.S. Macgregor, R.T.J. Moody, and D.D. Clark-Lowes, eds., Petroleum geology of North Africa: Geological Society, London, Special Publications 132, p. 109-129, doi: 10.1144/GSL.SP.1998.132.01.06.

Ehlers, T., T. Chaudhri, S. Kumar, C.W. Fuller, S.D. Willett, R.A. Ketcham, M.T. Brandon, D.X. Belton, B.P. Kohn, A.J.W. Gleadow, T.J. Dunai, and F.Q. Fu, 2005, Computational tools for low-temperature thermochronometer interpretation: Reviews in Mineralogy & Geochemistry, v. 58, p. 589-622, doi: 10.2138/rmg.2005.58.22.

English, J.M., 2012, Thermomechanical origin of regional fracture systems: AAPG Bulletin, v. 96, p. 1597-1625, doi: 10.1306/01021211018.

English, J.M., G.A. Lunn, L. Ferreira, and G. Yacu, 2015, Geologic evolution of the Iraqi Zagros, and its influence on the distribution of hydrocarbons in the Kurdistan region: AAPG Bulletin, v. 99, p. 231-272, doi: 10.1306/06271413205.

English, J.M., K.L. English, D.V. Corcoran, and F. Toussaint, 2016, Exhumation charge – the last gasp of a petroleum source rock and implications for unconventional gas: AAPG Bulletin, v. 100, doi: 10.1306/07271514224.

English, K.L., J. Redfern, G. Bertotti, J.M. English, and R. Yahia Cherif, in review A, Constraints on the geometry and magnitude of Cenozoic uplift in the Hoggar region of North Africa: Basin Research.

English, K.L., J.M. English, J. Redfern, C. Hollis, D.V. Corcoran, N. Oxtoby, and R. Yahia Cherif, in review B, Remobilization of deep basin brine during exhumation of the Illizi Basin, Algeria, Marine and Petroleum Geology.

Eschard, R., H. Abdallah, F. Braik, and G. Desaubliaux, 2005, The Lower Paleozoic succession in the Tasilli outcrops, Algeria: First Break, v. 23, p 27-36.

Fabre, J., 1976, Introduction à la géologie du Sahara algérien et des régions voisines: Algiers, Algeria, Sociétié Nationale d'Édition et de Diffusion, 422 p.

Fleischer, R.L., P.B. Price, and R.M. Walker, 1975, Nuclear Tracks in Solids: Berkeley, University of California Press, 605 p.

Galeazzi, S., O. Point, N. Haddadi, J. Mather, and D. Druesne, 2010, Regional geology and petroleum systems of the Illizi–Berkine area of the Algerian Saharan Platform: An overview: Marine and Petroleum Geology, v. 27, p 143-178, doi: 10.1016/j.marpetgeo.2008.10.002.

Ghienne, J.-F., D.P. Le Heron, J. Moreau, M. Denis, and M. Deynoux, 2007, The Late Ordovician glacial sedimentary system of the North Gondwana Platform, *in* M.J. Hambrey, P. Christoffersen, N.F. Glasser, and B. Hubbard, eds., Glacial sedimentary processes and products: Blackwell Publishing Ltd., Oxford, p. 295-319, doi: 10.1002/9781444304435.ch17.

Ghienne, J.-F., J. Moreau, L. Degermann, and J.-L. Rubino, 2013, Lower Palaeozoic unconformities in an intracratonic platform setting: glacial erosion versus tectonics in the eastern Murzuq Basin (southern Libya): International Journal of Earth Sciences, v. 102, p 455-482, doi: 10.1007/s00531-012-0815-y.

Goldstein, R.H., 2001, Fluid inclusions in sedimentary and diagenetic systems: Lithos, v. 55, p 159-193, doi: 10.1016/S0024-4937(00)00044-X.

Goldstein, R.H., and T.J. Reynolds, 1994, Systematics of fluid inclusions in diagenetic minerals: Society for Sedimentary Geology Short Course 31, 199 p.

Grabowski Jr., G.J., 2005, Sequence stratigrpahy and distribution of Silurian organic-rich "hot shales" of Arabia and North Africa: International Petroleum Technology Conference, IPTC-10388-ABSTRACT, doi: 10.2523/10388-ABSTRACT.

Green, P., and I. Duddy, 2012, Thermal history reconstruction in sedimentary basins using apatite fission-track analysis and related techniques, *in* N.B. Harris, and K.E. Peters, eds., Analyzing the thermal history of sedimentary basins: Methods and case studies: Society for Sedimentary Geology, Special Publication 103, p. 65-104.

Guiraud, R., W. Bosworth, J. Thierry, and A. Delplanque, 2005, Phanerozoic geological evolution of northern and central Africa: An overview: Journal of African Earth Sciences, v. 43, p. 83–143, doi: 10.1016/j.jafrearsci.2005.07.017.

Hanor, J.S., 1994, Origin of saline fluids in sedimentary basins, *in* J. Parnell, ed., Geofluids: origin, migration and evolution of fluids in sedimentary basins: Geological Society, London, Special Publication 78, p. 151-174, doi: 10.1144/GSL.SP.1994.078.01.13.

Hillis, R.R., 1995, Quantification of Tertiary exhumation in the United Kingdom southern North Sea using sonic velocity data: AAPG Bulletin, v. 79, p. 130-152.

Hirst, J. P., 2012, Ordovician proglacial sediments in Algeria: insights into controls on hydrocarbon reservoirs in the In Amenas field, Illizi basin, *in* M. Huuse, J. Redfern, D.P. Le Heron, R.J. Dixon, A. Moscariello, and J. Craig, eds., Glaciogenic Reservoirs and Hydrocarbon Systems: Geological Society, London, Special Publications 368, p. 319-353, doi: 10.1144/SP368.17.

Jacob, H., 1989, Classification, structure, genesis and practical importance of natural solid oil bitumen ("migrabitumen"): International Journal of Coal Geology, v. 11, p. 65–79, doi: 10.1016/0166-5162(89)90113-4.

Japsen, P., T. Mukerji, and G. Mavko, 2007, Constraints on velocity-depth trends from rock physics models: Geophysical Prospecting, v. 55, p. 135–154, doi: 10.1111/j.1365-2478.2007.00607.x.

Jarvie, D., B. Claxton, F. Henk, and J. Breyer, 2001, Oil and shale gas from the Barnett Shale, Fort Worth Basin, Texas: AAPG Annual Meeting Program, v.10, p.A100.

Jarvie, D.M., R.J. Hill, T.E. Ruble, and R.M. Pollastro, 2007, Unconventional shale-gas systems: The Mississippian Barnet shale of north central Texas as one model for thermogenic shale-gas assessment: AAPG Bulletin, v. 91, p. 475-499, doi: 10.1306/12190606068.

Katz, D., 1959, Handbook of Natural Gas Engineering: McGraw-Hill, New York, 705 p.

Kesler, S.E., M.S. Appold, A.M. Martini, L.M. Walter, T.J. Huston, and J.R. Kyle, 1995, Na-Cl-Br systematics of mineralizing brines in Mississippi Valley–type deposits: Geology, v. 23, p. 641-644, doi: 10.1130/0091-7613(1995)023<0641:NCBSOM>2.3.CO;2.

Ketcham, R.A., A. Carter, R.A. Donelick, J. Barbarand, and A.J. Hurford, 2007, Improved modelling of fission-track annealing in apatite: American Mineralogist, v. 92, p. 799-810, doi: 10.2138/am.2007.2281.

Konaté, M., J. Lang, M. Guiraud, M. Yahaya, M. Denis, and S. Alidou, 2006, Un bassin extensif formé pendant la fonte de la calotte glaciaire hirnantienne: le bassin ordovico-silurien de Kandi (Nord Bénin, Sud Niger): Africa Geoscience Review, v. 13, p. 157-183.

Lander, R., and O. Walderhaug, 1999, Predicting porosity through simulating sandstone compaction and quartz cementation: AAPG Bulletin, v. 83, p. 433-449.

Landis, C.R., and J.R. Castano, 1995, Maturation and bulk chemical properties of a suite of solid hydrocarbons: Organic Geochemistry, v. 22, no. 1, p. 137–149, doi: 10.1016/0146-6380(95)90013-6.

Lefranc, J.P., and R. Guiraud, 1990, The continental intercalaire of northwestern Sahara and its equivalents in the neighbouring regions: Journal of African Earth Sciences, v. 10, p. 27-77, doi: 10.1016/0899-5362(90)90047-I.

Legrand, P., 1985, Lower Paleozoic rocks of Algeria, *in* C.H. Holland, ed., Lower Paleozoic Rocks of the World v. 4, Lower Paleozoic of North-Western and West Central Africa: John Wiley and Sons, London, p. 5–89.

Legrand, P., 2003, Paléogéographie du Sahara algérien à l'Ordovicien terminal et au Silurien inférieur: Bulletin Société Géologique de France, v. 174, p. 19-32.

Le Heron, D.P., and J. Craig, 2008, First order reconstructions of a Late Ordovician Saharan ice sheet: Journal of the Geological Society, v. 165, p. 19-29, doi: 10.1144/0016-76492007-002.

Le Maux, T., B. Murat, A. Chauveau, M. Amamra, and K. Mesdour, 2006, The challenges of building up a geological and reservoir model of a Late Ordovician glaciomarine gas reservoir characterised by the presence of natural fractures: Society of Petroleum Engineers, SPE-101208-MS, doi: 10.2118/101208-MS.

Lesquer, A., D. Takherist, J.M. Dautria, and O. Hadiouche, 1990, Geophysical and petrological evidence for the presence of an "anomalous" upper mantle beneath the Sahara basins (Algeria): Earth and Planetary Science Letters, v. 96, p.407-418, doi: 10.1016/0012-821X(90)90016-Q.

Lewan, M.D., and T.E. Ruble, 2002, Comparison of petroleum generation kinetics by isothermal hydrous and nonisothermal open-system pyrolysis: Organic Geochemistry, v. 33, p. 1457-1475, doi: 10.1016/S0146-6380(02)00182-1.

Liégeois, J.P., A. Benhallou, A. Azzouni-Sekkal, R. Yahiaouni, and B. Bonin, 2005, The Hoggar swell and volcanism: Reactivation of the Precambrian Tuareg shield during Alpine convergence and West African Cenozoic volcanism, *in* G.R. Foulger, J.H. Natland, D.C. Presnall, and D.L. Anderson, eds., Plates, Plumes and Paradigms: Geological Society of America Special Paper 388, p. 379–400, doi: 10.1130/0-8137-2388-4.379.

Lüning, S., J. Craig, D.K. Loydell, P. Štorch, and B. Fitches, 2000, Lower Silurian 'hot shales' in North Africa and Arabia: regional distribution and depositional model: Earth Science Reviews, v. 49, p. 121-200, doi: 10.1016/S0012-8252(99)00060-4.

Macgregor, D.S., 1998, Giant fields, petroleum systems and exploration maturity of Algeria, *in* D.S. Macgregor, R.T.J. Moody, and D.D. Clark-Lowes, eds., Petroleum Geology of North Africa: Geological Society, London, Special Publications 132, p. 79-96, doi: 10.1144/GSL.SP.1998.132.01.04.

Makhous, M., Y.I. Galushkin, and N. Lopatin, 1997, Burial history and kinetic modeling for hydrocarbon generation; Part II, Applying the GALO model to Saharan basins: AAPG Bulletin, v. 81, p. 1679-1699.

Magara, K., 1976, Thickness of removed sedimentary rocks, paleopore pressure, and paleotemperature, southwestern part of Western Canada Basin: AAPG Bulletin, v. 60, p. 554–566.

Moreau, J., 2011, The Late Ordovician deglaciation sequence of the SW Murzuq Basin (Libya): Basin Research, v. 23, p. 449-477, doi: 10.1111/j.1365-2117.2010.00499.x.

Munz, I.A., 2001, Petroleum inclusions in sedimentary basins: systematics, analytical methods and applications: Lithos, v. 55, p. 195-212, doi: 10.1016/S0024-4937(00)00045-1.

Oakes, C.S., R.J. Bodnar, and J.M. Simonson, 1990, The system NaCl-$CaCl_2$-H_2O 1: The ice liquidus at 1 atm total pressure: Geochimica et Cosmochimica Acta, v. 54. p. 603-610, doi: 10.1016/0016-7037(90)90356-P.

Pepper, A.S., and P.J. Corvi, 1995, Simple kinetic models of petroleum formation. Part I: oil and gas generation from kerogens: Marine and Petroleum Geology, v. 12, p. 291-319, doi: 10.1016/0264-8172(95)98381-E.

Peters, K.E., and M.R. Cassa, 1994, Applied source rock geochemistry, *in* L.B. Magoon, and W.G. Dow, eds., The Petroleum System – From Source to Trap: Tulsa, AAPG Memoir 60, p. 93-120.

Peters, K.E., C.C. Walters, and J.M. Moldowan, 2005, The Biomarker Guide, Volume 1: Biomarkers and Isotopes in the Environment and Human History: Cambridge, UK, Cambridge University Press, 492 p.

Philippe, G., A.J.C. Cave, H. Khemissa, and B. Murat, 2003a, Late Ordovician (Unit IV Interval) reservoir characterization from the Ohanet/In Adaoui fields, Algeria (abs.): AAPG Search and Discovery, article 90016, http://www.searchanddiscovery.com/abstracts/pdf/2003/hedberg_algeria/allabstracts/ndx_Philippe01.pdf (accessed December 10th, 2014).

Philippe, M., G. Cuny, M. Bamford, E. Jaillard, G. Barale, B. Gomez, M. Ouaja, F. Thévenard, M. Thiébaut, and P. Von Sengbusch, 2003b, The palaeoxylological record of

Metapodocarpoxylon libanoticum (Edwards) Dupéron-Laudoueneix et Pons and the Gondwana Late Jurassic–Early Cretaceous continental biogeography: Journal of Biogeography, v. 30, p. 389-400, doi: 10.1046/j.1365-2699.2003.00835.x.

Pryor, W.A., 1973, Permeability–porosity patterns and variations in some Holocene sand bodies: AAPG Bulletin, v. 57, p. 162-189.

Rittenhouse, G., 1967, Bromine in oil-field waters and its use in determining possibilities of origin of these waters: AAPG Bulletin, v. 51, p. 2430-2440.

Roedder, E, 1984, Fluid inclusions: Mineralogical Society America, Reviews in Mineralogy, vol. 12, Washington, D.C., 644 p.

Rougier, S., Y. Missenard, C. Gautheron, J. Barbarand, H. Zeyen, R. Pinna, J.P. Liégeois, B. Bonin, A. Ouabadi, M. El-Messaoud Derder, and D. Frizon de Lamotte, 2013, Eocene exhumation of the Tuareg Shield (Sahara Desert, Africa): Geology, v. 41, p. 615-618, doi: 10.1130/G33731.1.

Roussé, S., S.E. Sandvik, B. Murat, A. Hutchinson, K. Saadi, and E. Le Guerroué, 2009, Depositional model and allostratigraphic architecture of Late Ordovician syn-glacial strata from the Tiguentourine Field (Illizi Basin, Algeria): Extended Abstract, 8th PESGB/HGS Conference on African E&P.

Rossi, C., O. Kälin, J. Arribas, and A. Tortosa, 2002, Diagenesis, provenance and reservoir quality of Triassic TAGI sandstones from Ourhoud field, Berkine (Ghadames) basin, Algeria: Marine and Petroleum Geology, v. 19, p. 117-142, doi: 10.1016/S0264-8172(02)00004-1.

Schoenherr, J., Littke, R., Urai, J., Kukla, P., and Rawahi, Z., 2007, Polyphase thermal evolution in the Infra-Cambrian Ara Group (South Oman Salt Basin) as deduced by maturity of solid reservoir bitumen: Organic Geochemistry, v. 38, p. 1293-1318, doi: 10.1016/j.orggeochem.2007.03.010.

Sclater, J.G., and P.A.F. Christie, 1980, Continental stretching: An explanation of the post-mid Cretaceous subsidence of the Central North Sea Basin: Journal of Geophysical Research, v. 85, no. B7, p. 3711-3739, doi: 10.1029/JB085iB07p03711.

Spaak, P., 2013, Silurian source rock system in time and space: International Petroleum Technology Conference, IPTC-16737, doi: 10.2523/16737-ABSTRACT.

Stampfli, G.M., and G.D. Borel, 2002, A plate tectonic model for the Paleozoic and Mesozoic constrained by dynamic plate boundaries and restored synthetic oceanic isochrons: Earth and Planetary Science Letters, v. 196, p. 17-33, doi: 10.1016/S0012-821X(01)00588-X.

Suárez-Ruiz, I., D. Flores, J. Granciano Mendonça Filho, and P.C. Hackley, 2012, Review and update of the applications of organic petrology: Part 1, geological applications: International Journal of Coal Geology, v. 99, p. 54-112, doi: 10.1016/j.coal.2012.02.004.

Sweeney, J.J., and A.K. Burnham, 1990, Evaluation of a simple model of vitrinite reflectance based on chemical kinetics: AAPG Bulletin, v. 74, p. 1559-1570.

Tissot, B., J. Espitalié, G. Deroo, C. Tempere, and D. Jonathan, 1984, Origin and Migration of Hydrocarbons in the Eastern Sahara (Algeria), *in* G. Demaison, and R.J. Murris, eds., Petroleum Geochemistry and Basin Evaluation: Tulsa, AAPG Memoir 35, p. 315-334.

Tissot, B.P., R. Pelet, and P.H. Ungerer, 1987, Thermal history of sedimentary basins, maturation indices, and kinetics of oil and gas generation: AAPG Bulletin, v. 71, p. 1445-1466.

Turner, P., D. Pilling, D. Walker, J. Exton, J. Binnie, N. Sabaou, 2001, Sequence stratigraphy and sedimentology of the late Triassic TAG-I (Blocks 401/402, Berkine Basin, Algeria), Marine and Petroleum Geology, v. 18, p. 959-981.

Turner, P., and H. Sherif, 2007, A giant late Triassic–Early Jurassic evaporitic basin on the Saharan Platform, North Africa, *in* B.C. Schreiber, S. Lugli, and M. Bąbel, eds., Evaporites Through Space and Time: Geological Society, London, Special Publications 285, p. 87-105, doi: 10.1144/SP285.6.

Underdown, R., 2006, An integrated basin modelling study of the Ghadames Basin, North Algeria: Ph.D. Thesis, University of Manchester, 609 p.

Underdown, R., and J. Redfern, 2008, Petroleum generation and migration in the Ghadames Basin, North Africa: A two-dimensional basin-modeling study: AAPG Bulletin, v. 92, p. 53-76, doi: 10.1306/08130706032.

Van de Weerd, A.A., and P.L.G. Ware, 1994, A review of the East Algerian Sahara oil and gas province (Triassic, Ghadames and Illizi Basins): First Break, v. 12, p. 363-373, doi: 10.3997/1365-2397.1994023.

Wagner, G.A., and P. Van den Haute, 1992, Fission-Track Dating: Kluwer Academic Publishers, Dordrecht, 285 p.

Walderhaug, O., 1994, Precipitation rates for quartz cement in sandstones determined by fluid-inclusion microthermometry and temperature history modeling: Journal of Sedimentary Research, v. 64, p. 324–333.

Walderhaug, O., 2000, Modeling quartz cementation and porosity in Middle Jurassic Brent Group sandstones of the Kvitebjorn field, northern North Sea: AAPG Bulletin, v. 84, p. 1325–1339, doi: 10.1306/A9673E96-1738-11D7-8645000102C1865D.

Walter, L.M., A.M. Stueber, and T.J. Huston, 1990, Br-Cl-Na systematics in Illinois basin fluids: Constraints on fluid origin and evolution: Geology, v. 18, p. 315-318, doi: 10.1130/0091-7613(1990)018<0315:BCNSII>2.3.CO;2.

Wilson, M., and R. Guiraud, 1992, Magmatism and rifting in Western and Central Africa, from Late Jurassic to Recent times: Tectonophysics, v. 213, p. 203–225, doi: 10.1016/0040-1951(92)90259-9.

Wilson, M., R. Guiraud, C. Moreau, and Y.J.C. Bellion, 1998, Late Permian to Recent magmatic activity on the African-Arabian margin of Tethys, *in* D.S. MacGregor, R.T.J. Moody, and D.D. Clark-Lowes, eds., Petroleum Geology of North Africa: Geological Society, London, Special Publication 132, p. 231-263, doi: 10.1144/GSL.SP.1998.132.01.14.

Wygrala, B.P., 1989, Integrated study of an oil field in the southern Po basin, northern Italy: Ph.D. thesis, Köln University, Research Centre Jülich, 217 p.

Yahi, N., 1999, Petroleum generation and migration in the Berkine (Ghadames) Basin, eastern Algeria: An organic geochemical and basin modelling study: Ph.D. thesis, Aachen University of Technology, 225 p.

Yahi, N., R.G. Schaefer, and R. Littke, 2001, Petroleum generation and accumulation in the Berkine Basin, eastern Algeria: AAPG Bulletin, v. 85, p. 1439-1467, doi: 10.1306/8626CAD7-173B-11D7-8645000102C1865D.

Yarmolyuk, V.A. and Y.Y. Kuznetsov, 1977, Geological map of Africa: Ministry of Geology of the USSR, Moscow, Russia, scale 1:5,000,000, 9 sheets.

Zeroug, S., N. Bounoua, and R. Lounissi, 2007, Well Evaluation Conference (WEC) Algérie 2007, Sonatrach-Schlumberger: Wetmore Printing Company, Houston, 536 p.

List of Tables

List of Figures

cross-section of the present-day Illizi and Berkine basins. The present-day post-Hercynian northward tilt of the Illizi Basin involves all of the Mesozoic section, including the post-Austrian stratigraphy. This tilting event is due to Cenozoic uplift of the Hoggar region and led to significant erosion in the southern Illizi Basin (English et al., in review A). Location of the study area (Well A) is projected along-strike into this section; note that the outcropping formation in the study area is Namurian and not Jurassic. The thermal maturity of the lower Silurian source rock (Daniels and Emme, 1995) decreases over the Ahara high due to thinning of the Paleozoic section, and over the Amguid-El Biod ridge due to increased Hercynian erosion. Both transects are modified from Galeazzi et al. (2010).

Figure 5: (A) Silurian isopach map (contours from Galeazzi et al., 2010). Along the western flank, the Silurian thickness is truncated due to Hercynian erosion. Within the Illizi Basin, there are pronounced Silurian thins over the Ahara high and the Isarene high. The ages of the basal Silurian shale immediately above the Ordovician are labelled (Lüning et al., 2000), including new data from the study area, which are dated as middle Telychian. The variation of Silurian basal shale ages indicates that the Isarene high was flooded approximately ~5 Ma later than the Tassili N'Ajjers region (upper Rhuddanian; Legrand, 1985). (B) A south to north well correlation of the lower Silurian shale interval indicates thinning of the basal shale onto the Isarene high. Hence, areas of thinner gross Silurian isopach correspond to younger basal Silurian graptolite ages confirming the diachronous Silurian onlap onto pre-existing topography. (C) Biostratigraphic data from Silurian graptolites are assigned to the *Streptograptus crispus* to *Monoclimacis griestoniensis* biozones.

Figure 6: (A) Velocity–depth plot of the Tournaisian and Devonian Frasnian shale intervals. The *C40* shale reference curve (from Dixon et al., 2010) was used for this analysis. The measured velocity of each shale interval was higher than the reference shale compaction curve indicating that these sequences are overcompacted. The *C50* shale reference curve was not used in this analysis, but it is illustrated, however, to communicate that although this technique provides a good estimate of relative changes in apparent exhumation, it has a poor resolution in estimating the absolute magnitude of exhumation, and requires calibration with other techniques. (B) Map of apparent exhumation across the study area using the average Tournaisian and Devonian shale intervals. The magnitude of overcompaction is greater in the south indicating greater burial

depths in the south (Well G) compared to the north (Well A). Black dots indicate wells used in the analysis. (C) Present-day Top Ordovician structure map (TVD bSRD: below seismic reference datum +400m [+1312 ft]). The Top Ordovician in Well G is only 22m [72 ft] deeper than in Well A present-day. (D) The maximum burial depth map of the Top Ordovician is the sum of maps B and C. The result causes the south to be 'pushed down' to account for the higher degree of exhumation compared to the north. In contrast with the present-day Top Ordovician structure, the maximum burial map opens up to the north suggesting the field area was, at this time, on the southern flank of a regional structural high. Well G is estimated to have been ~300-400 m [984-1312 ft] deeper than Well A at peak burial using this technique.

Figure 7: (A) Thermal maturity data from Well A, Well E and Well H in the northern part of the field. Present-day thermal maturity is higher than what would be expected from current burial depths (default maturity profile shown by dashed red line) indicating that these rocks have been hotter in the past. (B) Indicative peak paleotemperatures estimated from maturity data using *Easy%*R_o (Sweeney and Burnham, 1990), and assuming a heating rate of 1°C/Myr. This graph also serves to illustrate the broad similarity between the estimated paleogeothermal gradient at maximum burial and the present-day geothermal gradient.

Figure 8: Lower Silurian thermal maturity data superimposed on the sonic compaction-derived maximum burial map for the Base Silurian/Top Ordovician. Maturity data and sonic compaction analysis independently illustrate the presence of a regional paleostructure to the north of the field that persisted until maximum burial. Peak burial temperatures from the north to south differ by ~15-20°C [27-36°F], which is supported by both methods. Maturity values are an average of vitrinite and equivalents (including Rock-Eval pyrolysis data) for individual wells. Control points in italics represent Silurian maturity estimates extrapolated from Devonian Rock-Eval pyrolysis data in offsetting wells. Note: There are two available maturity estimates for the lower Silurian in Well F, and the higher value* is adopted here.

Figure 9: Summary of Upper Ordovician homogenization temperatures (T_h) from primary and secondary aqueous and petroleum inclusions. The first-formed low-salinity aqueous inclusions indicate modal T_h between 135-145°C [275-293°F] in Well A (Panel A) and 140-155°C [284-311°F] in Well G (Panel C). The later high-salinity (>18 wt.%) aqueous inclusions mostly occur over a cooler temperature range of 85-120°C [185-248°F] (Panels B and E), and are interpreted

to have formed during exhumation and cooling. An intermediate-salinity (9-16 wt.%) group, with intermediate T_h, was found in Well G (Panel D), and may represent the transition between the two end-member salinity groups. Primary oil inclusions trapped at peak temperatures (F, green columns), contain a range of 34-42° API gravity, while later primary oil and aqueous oil-associated inclusions (Panels B and F, black columns), formed at cooler temperatures in late barite cement, and correspond to a gravity of 46° API. The higher-temperature, quartz-hosted, primary petroleum inclusions are characterized by single-phase oil, while the lower-temperature, barite-hosted, primary petroleum inclusions are characterized by phase-separated oil and gas. The gravity range from the secondary inclusions is 36-46° API and represents the full spectrum of temperatures (Panel G).

Figure 10: Example of a quartz grain and quartz overgrowth from the Upper Ordovician in Well D showing the relationship between primary and secondary inclusions. Higher salinity (17.2 wt.%) secondary aqueous inclusions within a healed microfracture cross-cut the quartz overgrowth and quartz grain, which contain primary inclusions of lower salinity (7-8 wt.%) formed at higher temperatures (145-170°C [293-338°F]). (Photo by N. Oxtoby).

Figure 11: Actual measured fission-track ages (red circles) versus stratigraphic age according to depth (modified from English et al., in review A). All samples provide fission-track ages that are younger than depositional ages, and show a trend of decreasing fission-track age with depth due to greater degree of annealing. The default profile illustrates the predicted fission-track ages (for apatites with 0.1 wt.% chlorine content) assuming no additional burial. The measured fission-track ages are routinely younger than the default profile, and suggest that this stratigraphic sequence has experienced hotter temperatures in the past. The continuous 'Well A Model' profile of fission-track age was generated via forward modelling of the final Well A thermal history model assuming a chlorine content of 0.1 wt.%. Actual samples with higher chlorine contents will be more resistant to annealing for a given thermal history, and forward modelling of the actual fission-track samples (blue squares) may plot off of the continuous profile. The final Well A thermal history model provides a much better fit to the measured fission-track ages. Fission-track modelling was carried out with *HeFTy* using the annealing kinetics of Ketcham et al. (2007).

Figure 12: 1D burial history models for Well A and Well G.

Figure 13: Thermal history profiles for the Top Ordovician for Well A and Well G. Peak paleotemperature for the Top Ordovician is estimated at 140°C [284°F] in Well A and 156°C [313°F] in Well G.

Figure 14: Graph showing the Silurian source rock temperature, transformation ratio (TR) and volume of oil and gas expelled for Well A and Well G. Well G produces more hydrocarbons due to greater thermal exposure. Oil expulsion occurs first in the south of the field (Well G) followed by the north (Well A) during the Carboniferous. Relatively minor volumes of oil and gas are also expelled during the second phase of burial in the Late Cretaceous to early Eocene. Trap formation occurred after the second phase of hydrocarbon generation.

Figure 15: Comparison between (A) Top Ordovician peak burial map based on sonic overcompaction analysis (same as Fig. 6D) and (B) Top Ordovician peak burial map derived by reversing the Cenozoic uplift via tilting the present-day structure map. Both independent techniques indicate that the Ordovician field was located on a southward-plunging structural nose during early Eocene peak burial, and that the present-day structural closure was formed during the Cenozoic uplift event associated with the Hoggar swell.

Figure 16: Petroleum systems event chart for the Ordovician play in the Illizi Basin.

Figure 17: Expulsion sensitivity analysis as a function of magnitude of Cenozoic exhumation. Hydrocarbon generation and expulsion is significantly decreased for exhumation magnitudes in excess of 300 m [984 ft]. In this study, Cenozoic exhumation is estimated at 1230 m [4035 ft] at Well A in the Illizi Basin, where Namurian strata crop out.

TABLE 1: NEW BASAL SILURIAN HOT SHALE GRAPTOLITE BIOSTRATIGRAPHY (THIS STUDY)

WELL	Interval	*Metaclimacograptus flamandi*	*'Monograptus'? sp.*	*Monograptus priodon*	*Monograptus marri*	*Parapetalolithus meridionalis*	*Pseudoplegmatograptus obesus*	*Retiolites angustidens*	*Spirograptus turriculatus*	*Stimulograptus sp.*	*Streptograptus exiguus*	*Streptograptus sartorius*	*Torquigraptus sp.*	*Torquigraptus arcuatus*	*Torquigraptus australis*
Well D	1912.26-1912.32 m	x		x											
	1916.81-1916.88 m	x												x	
	1920.00-1920.08 m	x		x	x				x	x	x				
	Biozone	*Streptograptus crispus* in lowermost sample													
	Age	middle Telychian													
Well E	1963.7-1963.8 m	x				x	x						x		
	Biozone	*Streptograptus crispus* to *Monoclimacis griestoniensis*													
	Age	middle Telychian													
Well Z	2029.17 m		x?					x				x			x
	2036.0 m					x									
	Biozone	*Streptograptus crispus* to *Monoclimacis griestoniensis* in lower sample													
	Age	middle Telychian													

Analysis conducted by D. Loydell, University of Portsmouth

TABLE 2: NEW REFLECTANCE DATA (THIS STUDY)

Well	Analyst	Formation	Depth Interval		R_o Indicator	Sample Count	Vitrinite Reflectance	Bitumen or Chitinozoan Reflectance	Std Dev	Vit. Refl. Equiv.	Indicative peak paleo-temperature (°C)
			From (m)	To (m)			R_o-Random *($*R_o$-Max)*				
Well A	EGS	Namurian	195	350	V	8	0.63	-	0.07	-	104
Well A	EGS	Visean C	450	540	V	12	0.62	-	0.07	-	102
Well A	KK	Tournaisian	720	770	V	10	*(0.61*)*	-	0.05	-	101
Well A	EGS	Tournaisian	800	885	V	9	0.62	-	0.04	-	102
Well A	EGS	Devonian F2	990	1105	V	10	0.67	-	0.05	-	110
Well A	EGS	Devonian MPR	1110	1205	V	7	0.69	-	0.03	-	113
Well A	EGS	Devonian F3	1235	1330	V	14	0.72	-	0.07	-	117
Well A	KK	Devonian F4	1330	1350	V	13	*(0.67*)*	-	0.05	-	110
Well A	EGS	Upper Silurian	1665	1800	B	8	-	0.78	0.05	0.97	142
Well A	EGS	Lower Silurian	1800	1900	B	9	-	0.84	0.07	1.03	146
Well C	EGS	Tournaisian	660	780	V	10	0.52	-	0.10	-	89
Well C	KK	Devonian F2	780	800	V	10	*(0.86*)*	-	0.08	-	134
Well C	EGS	Devonian MPR	1010	1110	V	8	0.61	-	0.03	-	101
Well C	EGS	Devonian F3	1140	1240	V	10	0.62	-	0.05	-	102
Well C	KK	Devonian F4	1250	1270	V	14	*(0.86*)*	-	0.06	-	134
Well C	KK	Devonian F6C3	1320	1360	V	10	*(0.83*)*	-	0.07	-	131
Well C	EGS	Devonian F6 Shale	1535	1565	V	6	0.99	-	0.04	-	143
Well C	EGS	Upper Silurian	1615	1750	V	6	1.02	-	0.08	-	145
Well E	EGS	Namurian	160	170	V	12	0.68	-	0.05	-	112
Well E	EGS	Visean C	510	520	V	13	0.64	-	0.06	-	105
Well E	EGS	Tournaisian	730	740	V	13	0.67	-	0.07	-	110
Well E	EGS	Tournaisian	880	890	V	15	0.69	-	0.04	-	113
Well E	EGS	Lower Silurian	1730	1735	C	12	-	0.84	0.08	0.86	134
Well F	EGS	Visean C	290	300	V	13	0.66	-	0.06	-	109
Well F	EGS	Visean C	450	460	V	12	0.72	-	0.06	-	117
Well F	EGS	Tournaisian	640	650	V	11	0.63	-	0.05	-	104
Well F	EGS	F6C2 shale	1405	1410	V	12	0.67	-	0.05	-	110
Well F	EGS	Lower Silurian	1845	1850	C	10	-	1.27	0.06	1.27	160
Well F	EGS	Lower Silurian	1940	1945	C	10	-	1.13	0.06	1.14	152
Well G	EGS	Visean C	190	200	V	13	0.70	-	0.03	-	114
Well G	EGS	Visean B	480	490	V	10	0.83	-	0.05	-	131
Well G	EGS	Tournaisian	590	595	V	15	0.90	-	0.05	-	137
Well G	EGS	Devonian F2	775	780	V	13	0.94	-	0.07	-	140
Well G	EGS	F6C2	1380	1385	V	11	0.76	-	0.05	-	123
Well G	EGS	F6C2	1415	1420	V	7	0.81	-	0.05	-	129
Well G	EGS	F6M2	1580	1585	C	12	-	0.94	0.05	0.96	142
Well G	EGS	Lower Silurian	1930	1935	C	10	-	1.34	0.07	1.34	163
Well H	EGS	Namurian	190	200	V	9	0.73	-	0.04	-	119
Well H	EGS	Visean C	440	450	V	11	0.70	-	0.07	-	114
Well H	EGS	Tournaisian	930	940	V	11	0.75	-	0.05	-	122

Notes: Reflectance data were measured by two different contractors (KK = Keiraville Konsultants and EGS = Egs-ploration). No sample count exceeds 15 measurements due to limited sample volume, so the maturity estimates must be treated with some caution. Only samples with >5 measurements are provided here. Some Devonian samples with anomalously low reflectance were excluded due to suspected suppression. Measured indicators include: V= vitrinite; B = bitumen; C= chitinozoan. Measured solid bitumen reflectance was converted to R_o equivalent using an equation from Schoenherr et al. (2007): [$R_{vit} = (R_{bit} + 0.2433) / 1.0495$]. Measured chitinozoan reflectance was converted to R_o% equivalent using an equation from Alpern (1970): [$R_{vit} = (0.9612 * R_{chit}) + 0.0521$]. Vitrinite reflectance values (and equivalents) were converted to indicative maximum paleo-temperature estimates assuming a heating rate of 1°C/Myr (Sweeney and Burnham, 1990). This is close to the modelled heating rate for the Paleozoic burial history, where the Silurian source rock temperature increases 131°C over a period of 156 Myr (0.84°C/Myr) from the time of deposition to the time of Hercynian exhumation (Fig. 12).

TABLE 3: NEW ROCK-EVAL PYROLYSIS DATA (THIS STUDY)

Well	Sample Type	Formation	Depth (m)		TOC	S_1	S_2	S_3	T_{max}	HI	OI	GP	PI	Calc.	Calc. TR
			From	To	(wt.%)	mg_{HC}/g_{rock}	mg_{HC}/g_{rock}	mg_{HC}/g_{rock}	°C	mg_{HC}/g_{TOC}	mg_{CO2}/g_{TOC}	mg_{HC}/g_{rock}		Ro% eqv.	%
Well A	cuttings	Devonian F2	990	1105	1.67	0.39	3.92	0.64	438	235	38	4.31	0.09	0.72	60
Well A	cuttings	Devonian MPR	1110	1205	1.69	0.65	4.52	0.57	439	267	34	5.17	0.13	0.74	53
Well A	cuttings	Devonian F3	1235	1330	1.26	0.50	3.29	0.46	445	261	37	3.79	0.13	0.85	55
Well C	cuttings	Devonian F2	870	1000	1.51	0.81	3.81	0.54	442	252	36	4.62	0.18	0.80	57
Well C	cuttings	Devonian MPR	1010	1110	1.36	1.23	4.10	0.39	441	301	29	5.33	0.23	0.78	48
Well E	cuttings	Visean C	525	530	2.11	0.10	1.14	2.01	426	54	8	1.24	0.08	0.51	*92**
Well F	cuttings	Devonian F2	845	850	1.02	0.08	0.68	0.96	433	67	11	0.76	0.11	0.63	*90**
Well H	cuttings	Devonian F2	955	960	2.04	0.63	1.59	1.86	435	78	28	2.22	0.04	0.67	*88**
Well D	core	Lower Silurian	1920.8		14.40	2.68	12.83	0.31	462	89	2	15.51	0.17	1.16	93
Well E	core	Lower Silurian	1954.5		5.19	2.15	5.95	0.29	448	115	6	8.10	0.27	0.90	91
Well E	core	Lower Silurian	1955.7		8.33	3.22	10.22	0.49	450	123	6	13.44	0.24	0.94	90
Well E	core	Lower Silurian	1956.8		2.40	1.10	2.58	0.25	456	108	10	3.68	0.30	1.05	91

Notes: TOC: total organic carbon; S_1: hydrocarbon distilled by pyrolysis; S_2: hydrocarbon cracked from kerogen during pyrolysis; S_3: carbon dioxide generated during pyrolysis; T_{max}: temperature at maximum S_2 peak; HI: hydrogen index (S_2/TOC); OI: oxygen index (S_3/TOC); GP: genetic potential ($S_1 + S_2$); PI: production index (S_1/GP). Rock-Eval data were screened according to criteria of English et al. (2015) and Peters and Cassa (1994). The S_1 and S_2 peaks in the pyrograms were well defined in all samples except Well A (1235-1330m) and Well E (1956.8m), which showed a defined S_1 with a slightly broader S_2; both samples still passed the screening criteria. The T_{max} to R_o% conversion is from Jarvie et al. (2001) and Peters et al. (2005): [R_o*% eqv=(0.018*T_{max}) - 7.16*]. The Transformation Ratios (TR) were calculated according to Jarvie et al. (2007) assuming an original PI of 0.02, and an original HI of 630 mg_{HC}/g_{TOC} and 450 mg_{HC}/g_{TOC} for the Silurian core and Devonian-Carboniferous cuttings samples respectively. *Three of the calculated TRs from the cuttings samples appear to be anomalously high compared to the thermal maturity; this is likely due to the original HI for these samples being lower than the assumed value of 450 mg_{HC}/g_{TOC}.

TABLE 4: STRATIGRAPHIC INPUTS FOR WELL A & WELL G 1D BURIAL HISTORY MODELS

Formation	End of Event (Ma)	Thickness		Lithology	PWD (m)	Surface Temp. (°C)
		Well A	Well G			
RECONSTRUCTED STRATIGRAPHY						
Quaternary	0	0	0	-	0	22
	16	*-555*	*-690*	-	*0*	*22*
Eocene-Miocene	*28*	*-195*	*-330*	-	*0*	*22*
Erosion	*31.4*	*-130*	*-270*	-	*0*	*22*
	47	*-350*	*-490*	-	*45*	*24*
Ypresian	52	75	75	sandstone, shale	50	24
Paleocene	56	75	75	shale, limestone	75	24
Senonian Carbonate	66	75	75	shale, limestone	75	25
Senonian Anhydrite	78	55	55	shale, limestone, anhydrite	75	26
Senonian Salifere	86.3	30	30	limestone, shale, gypsum, anhydrite	50	26
Turonian	89.8	70	70	limestone	50	27
Cenomanian Limestone	93.9	35	35	shale, limestone	50	27
Cenomanian Argile a Gypse	95	70	70	shale, gypsum, limestone, anhydrite	50	27
Cenomanian D'In Akamil	98	60	60	limestone, shale	50	27
Albian	108	75	100	sandstone, shale	50	28
Aptian	113	15	15	limestone, shale	50	28
Austrian Erosion	*119*	*-50*	*-50*	-	*50*	*28*
Barremian	124	225	250	sandstone, shale	0	28
Neocomian	139	70	120	sandstone, shale	0	28
Upr Jurassic Malm	145	100	100	shale, sandstone, limestone	0	28
Mid Jurassic Dogger Argileux	163.5	20	20	shale	0	27
Mid Jurassic Dogger Lagunaire	168.3	25	25	sandstone, shale, limestone	5	25
Lower Jurassic Liassic	174.1	0	0	shale, limestone, salt	5	25
Triassic	201.3	0	0	sandstone	5	25
Hercynian Erosion	*231*	*-475*	*-425*	-	*0*	*28*
Permian	286	50	175	sandstone	0	23
Tiguentourine	298.9	450	460	shale, silt, gypsum	0	20
Westphalian F	303.9	80	140	sandstone, shale, limestone	0	19
Westphalian E	306	100	200	sandstone, shale, limestone	0	18
Namurian (Well G only)	313	0	105	sandstone, silt, shale, limestone	0	18
PRESERVED STRATIGRAPHY						
Westphalian	309	134	0	sandstone, silt, shale, limestone	0	18
Namurian	316	220	161	sandstone, silt, shale, limestone	0	17
Visean C	326	193	227	sandstone, shale	10	13
Visean B	339	157	179	sandstone, shale, limestone	15	10
Tournaisian	347	76	83	sandstone, silt, shale	20	12
Tournaisian Shale	352	112	135	shale	20	14
Devonian F2 sst	359	87	85	sandstone, shale	20	14
Devonian F2 Shale	363	133	113	shale	20	14
MPR	372	100	159	shale	20	7
Frasnian Erosion	*376*	*-10*	*-10*	-	*100*	*7*
Devonian F3 sst	381	34	29	sandstone, shale	100	6
Devonian F3 Shale	385	95	97	shale	100	6
Devonian F4 sst	388	20	38	sandstone, shale	50	7
Devonian F4 Shale	393	26	34	shale	40	7
Devonian F6C3	408	50	53	sandstone, shale	30	8
Devonian F6C2	409	18	39	sandstone, shale	20	9
Devonian F6C1	411	89	91	sandstone, shale	15	9
Caledonian Erosion	*417*	*-50*	*-50*	-	*15*	*10*
Silurian F6A Shale	419	97	94	sandstone, shale	15	10
Silurian F6M2 Shale	423	39	39	sandstone, shale	15	10
Silurian F6M1 Shale	426	48	71	sandstone, shale	20	9
Gothlandian Shale	427	210	254	shale	30	7
Silurian Lwr Hot Shale	441	37	16	shale	30	6
Ordovician Unit IV-3	442	12	37	shale	100	4
Ordovician IV	443	113	77	sandstone, silt, shale	10	5
Ordovician III-3	445	230	125	sandstone, silt	10	5
Lower Ordovician	470	30	48	sandstone, silt, shale	5	3
Cambrian	485	200	212	sandstone, silt, shale	5	8
base	541					

Preserved stratigraphy is present up to the Namurian-Westphalian. Reconstructed stratigraphy based on published and unpublished offset well data to north, west and east of the study area. Thicknesses of eroded Mesozoic and Carboniferous sediments during Eocene are tabulated in initial depositional thickness (uncompacted). Exhumation estimates quoted in text refer to compacted stratigraphy.

TABLE 5: MAIN LITHOTYPES AND PETROPHYSICAL PROPERTIES USED IN 1D BURIAL HISTORY MODELS

Lithology	Solid Density (g/cm^3)	Initial Porosity (%)	Thermal Conductivity (W/m/°K) at 20°C
Sandstone	2.65	40	3.85
Shale	2.72	60	1.62
Siltstone	2.65	50	3.35
Limestone	2.71	35	2.93
Gypsum	2.32	2	1.46
Anhydrite	2.96	2	5.02
Halite	2.17	2	5.86

Mass heat capacity = 837 (J/kg/°C) for all lithologies. Radioactivity (W/m^3) = $1.5*10^{-5}$ for shale.

TABLE 6: KINETIC ASSUMPTIONS FOR THE SILURIAN SOURCE ROCK

Source Rock Parameters		Value	Data Source
Kerogen Type		II	*Cole et al. (2000)*
Average TOC (initial) (%)		15	*Yahi (1999)*
HI (initial) (mg_{HC}/g_{TOC})		630	*Makhous et al. (1997)*
OIL	Activation Energy (kJ)	215.2	*Organofacies B; Pepper and Corvi (1995)*
	Frequency Factor (1/s)	8.14E+13	
GAS	Activation Energy (kJ)	278.7	
	Frequency Factor (1/s)	2.17E+18	

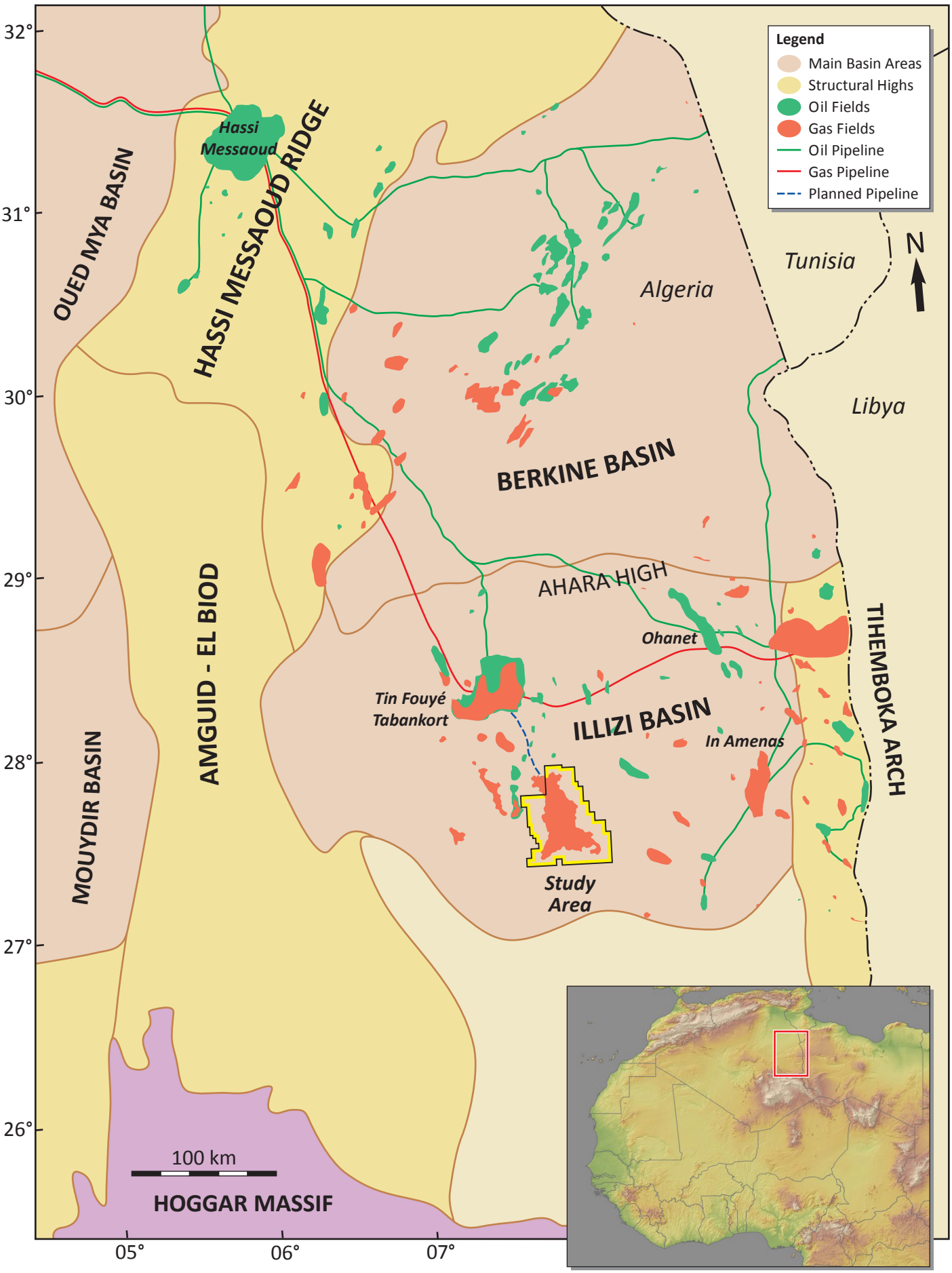
Legend
Main Basin Areas
Structural Highs
Oil Fields
Gas Fields
Oil Pipeline
Gas Pipeline
Planned Pipeline
N
Tunisia
Algeria
Libya
OUED MYA BASIN
HASSI MESSAOUD RIDGE
Hassi Messaoud
BERKINE BASIN
AHARA HIGH
Ohanet
Tin Fouyé Tabankort
ILLIZI BASIN
In Amenas
TIHEMBOKA ARCH
AMGUID - EL BIOD
MOUYDIR BASIN
Study Area
HOGGAR MASSIF
100 km
32°
31°
30°
29°
28°
27°
26°
05°
06°
07°

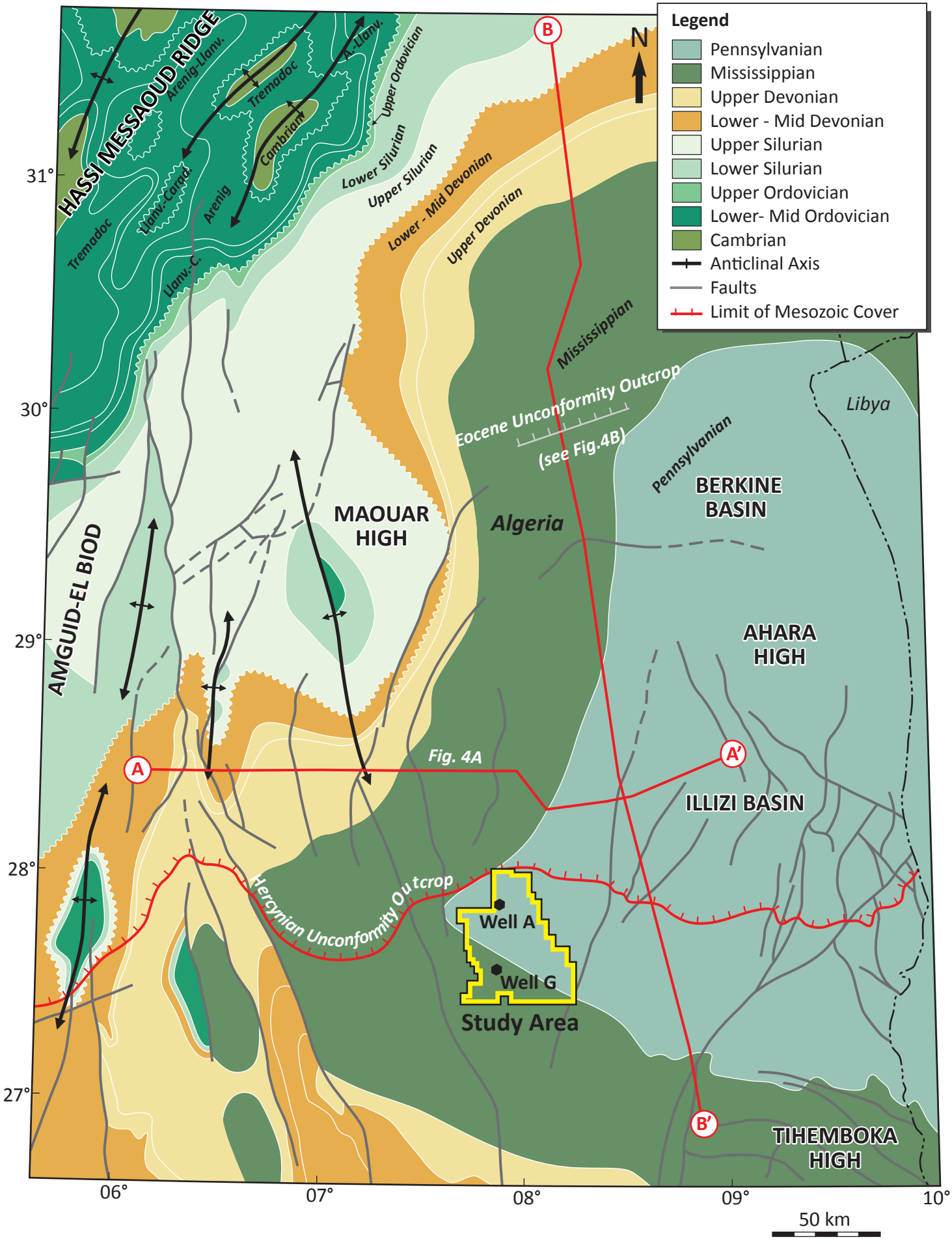
Legend
Pennsylvanian
Mississippian
Upper Devonian
Lower - Mid Devonian
Upper Silurian
Lower Silurian
Upper Ordovician
Lower- Mid Ordovician
Cambrian
Anticlinal Axis
Faults
Limit of Mesozoic Cover
N
HASSI MESSAOUD RIDGE
Arenig-Llanv.
Tremadoc
A.-Llanv.
Upper Ordovician
Cambrian
Lower Silurian
Upper Silurian
Lower - Mid Devonian
Upper Devonian
Llanv.-Carad.
Arenig
Llanv.-C.
Mississippian
Eocene Unconformity Outcrop
(see Fig.4B)
Libya
Pennsylvanian
BERKINE BASIN
MAOUAR HIGH
Algeria
AMGUID-EL BIOD
AHARA HIGH
Fig. 4A
A
A'
ILLIZI BASIN
Hercynian Unconformity Outcrop
Well A
Well G
Study Area
B
B'
TIHEMBOKA HIGH
31°
30°
29°
28°
27°
06°
07°
08°
09°
10°
50 km

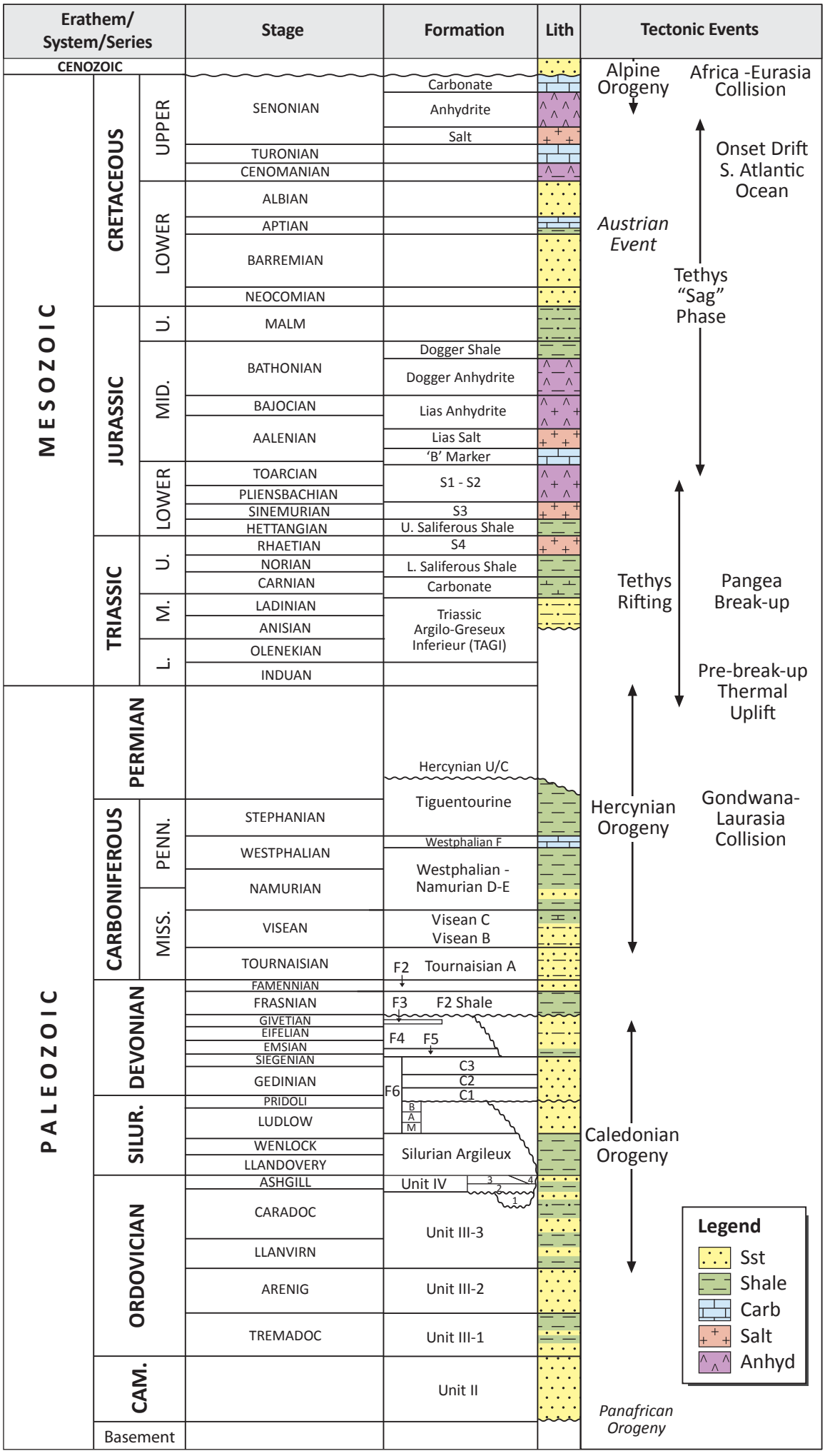
Erathem/ System/Series
Stage
Formation
Lith
Tectonic Events
CENOZOIC
MESOZOIC
CRETACEOUS
UPPER
LOWER
JURASSIC
U.
MID.
LOWER
TRIASSIC
U.
M.
L.
PALEOZOIC
PERMIAN
CARBONIFEROUS
PENN.
MISS.
DEVONIAN
SILUR.
ORDOVICIAN
CAM.
Basement
SENONIAN
TURONIAN
CENOMANIAN
ALBIAN
APTIAN
BARREMIAN
NEOCOMIAN
MALM
BATHONIAN
BAJOCIAN
AALENIAN
TOARCIAN
PLIENSBACHIAN
SINEMURIAN
HETTANGIAN
RHAETIAN
NORIAN
CARNIAN
LADINIAN
ANISIAN
OLENEKIAN
INDUAN
STEPHANIAN
WESTPHALIAN
NAMURIAN
VISEAN
TOURNAISIAN
FAMENNIAN
FRASNIAN
GIVETIAN
EIFELIAN
EMSIAN
SIEGENIAN
GEDINIAN
PRIDOLI
LUDLOW
WENLOCK
LLANDOVERY
ASHGILL
CARADOC
LLANVIRN
ARENIG
TREMADOC
Carbonate
Anhydrite
Salt
Dogger Shale
Dogger Anhydrite
Lias Anhydrite
Lias Salt
'B' Marker
S1 - S2
S3
U. Saliferous Shale
S4
L. Saliferous Shale
Carbonate
Triassic Argilo-Greseux Inferieur (TAGI)
Hercynian U/C
Tiguentourine
Westphalian F
Westphalian - Namurian D-E
Visean C
Visean B
F2 Tournaisian A
F3 F2 Shale
F4 F5
F6
C3
C2
C1
B
A
M
Silurian Argileux
Unit IV
3
2
4
1
Unit III-3
Unit III-2
Unit III-1
Unit II
Alpine Orogeny
Africa -Eurasia Collision
Onset Drift S. Atlantic Ocean
Austrian Event
Tethys "Sag" Phase
Tethys Rifting
Pangea Break-up
Pre-break-up Thermal Uplift
Hercynian Orogeny
Gondwana-Laurasia Collision
Caledonian Orogeny
Panafrican Orogeny
Legend
Sst
Shale
Carb
Salt
Anhyd

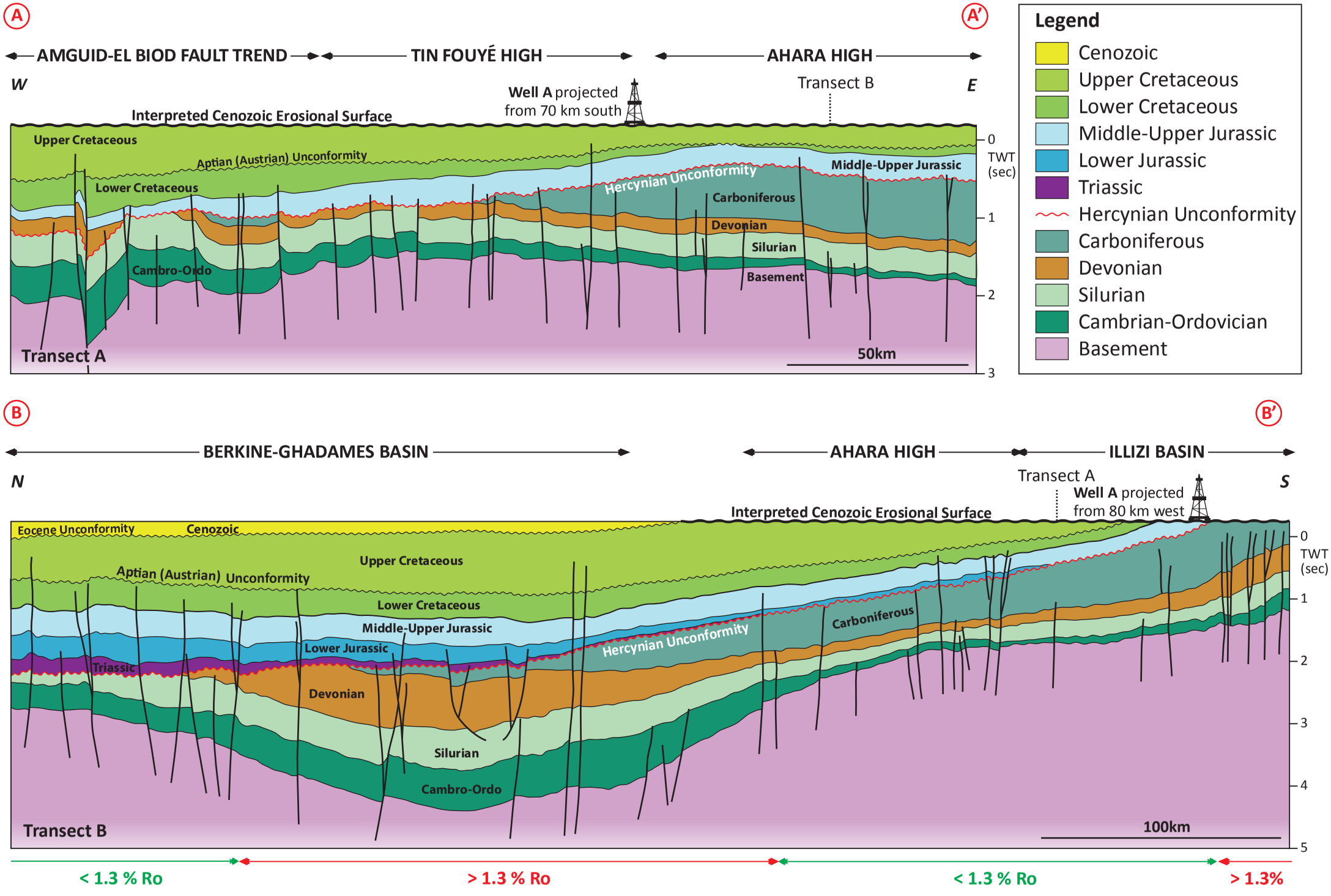

Lower Silurian Peak Maturity (based on Daniels and Emme, 1995)

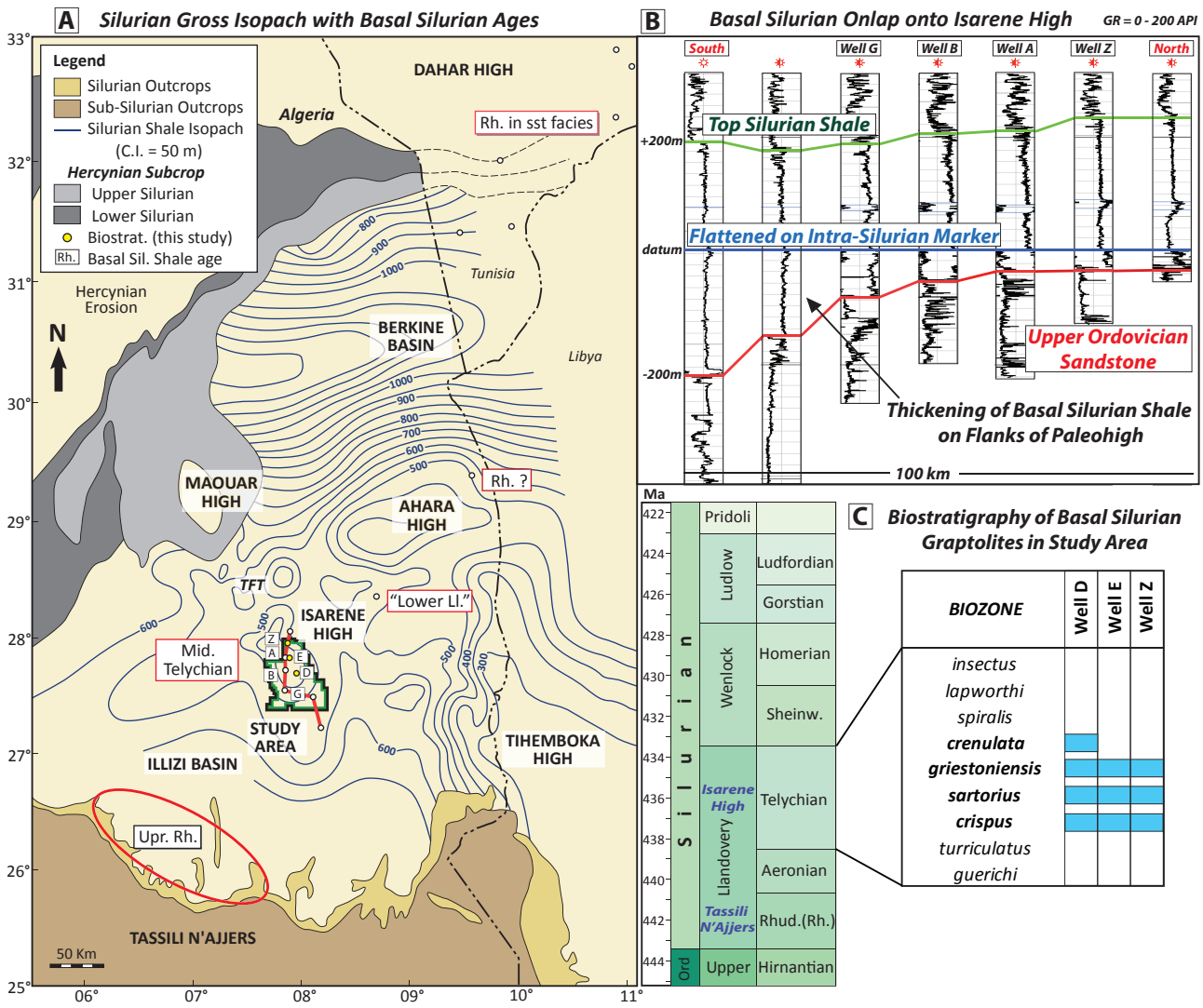
A
Silurian Gross Isopach with Basal Silurian Ages
Legend
Silurian Outcrops
Sub-Silurian Outcrops
Silurian Shale Isopach
(C.I. = 50 m)
Hercynian Subcrop
Upper Silurian
Lower Silurian
Biostrat. (this study)
Basal Sil. Shale age
DAHAR HIGH
Algeria
Rh. in sst facies
Tunisia
Hercynian Erosion
N
BERKINE BASIN
Libya
MAOUAR HIGH
AHARA HIGH
Rh. ?
TFT
"Lower Ll."
ISARENE HIGH
Mid. Telychian
STUDY AREA
ILLIZI BASIN
TIHEMBOKA HIGH
Upr. Rh.
TASSILI N'AJJERS
50 Km
33°
32°
31°
30°
29°
28°
27°
26°
25°
06°
07°
08°
09°
10°
11°
B
Basal Silurian Onlap onto Isarene High
GR = 0 - 200 API
South
Well G
Well B
Well A
Well Z
North
Top Silurian Shale
+200m
datum
Flattened on Intra-Silurian Marker
-200m
Upper Ordovician Sandstone
Thickening of Basal Silurian Shale on Flanks of Paleohigh
100 km
Ma
422
424
426
428
430
432
434
436
438
440
442
444
Silurian
Ord
Pridoli
Ludlow
Wenlock
Llandovery
Isarene High
Tassili N'Ajjers
Ludfordian
Gorstian
Homerian
Sheinw.
Telychian
Aeronian
Rhud.(Rh.)
Hirnantian
Upper
C
Biostratigraphy of Basal Silurian Graptolites in Study Area
BIOZONE
Well D
Well E
Well Z
insectus
lapworthi
spiralis
crenulata
griestoniensis
sartorius
crispus
turriculatus
guerichi

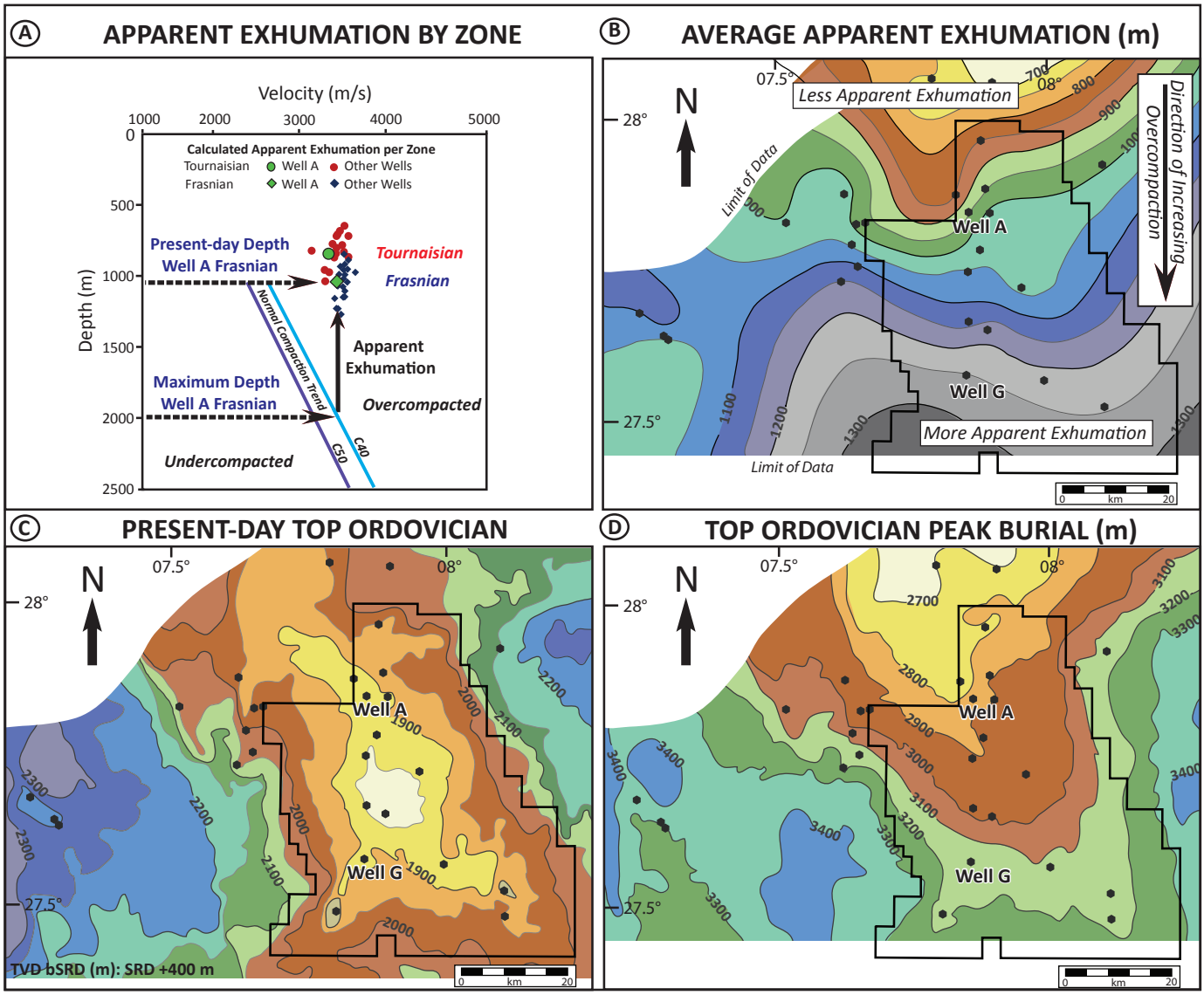
A
APPARENT EXHUMATION BY ZONE
Velocity (m/s)
1000
2000
3000
4000
5000
0
500
1000
1500
2000
2500
Depth (m)
Calculated Apparent Exhumation per Zone
Tournaisian
Well A
Other Wells
Frasnian
Well A
Other Wells
Present-day Depth
Well A Frasnian
Tournaisian
Frasnian
Normal Compaction Trend
C40
C50
Apparent
Exhumation
Maximum Depth
Well A Frasnian
Overcompacted
Undercompacted
B
AVERAGE APPARENT EXHUMATION (m)
07.5°
08°
28°
27.5°
N
Less Apparent Exhumation
Limit of Data
700
800
900
1000
1100
1200
1300
Well A
Well G
More Apparent Exhumation
Limit of Data
Direction of Increasing
Overcompaction
0
km
20
C
PRESENT-DAY TOP ORDOVICIAN
07.5°
08°
28°
27.5°
N
Well A
Well G
1900
2000
2100
2200
2300
TVD bSRD (m): SRD +400 m
0
km
20
D
TOP ORDOVICIAN PEAK BURIAL (m)
07.5°
08°
28°
27.5°
N
2700
2800
2900
3000
3100
3200
3300
3400
Well A
Well G
0
km
20

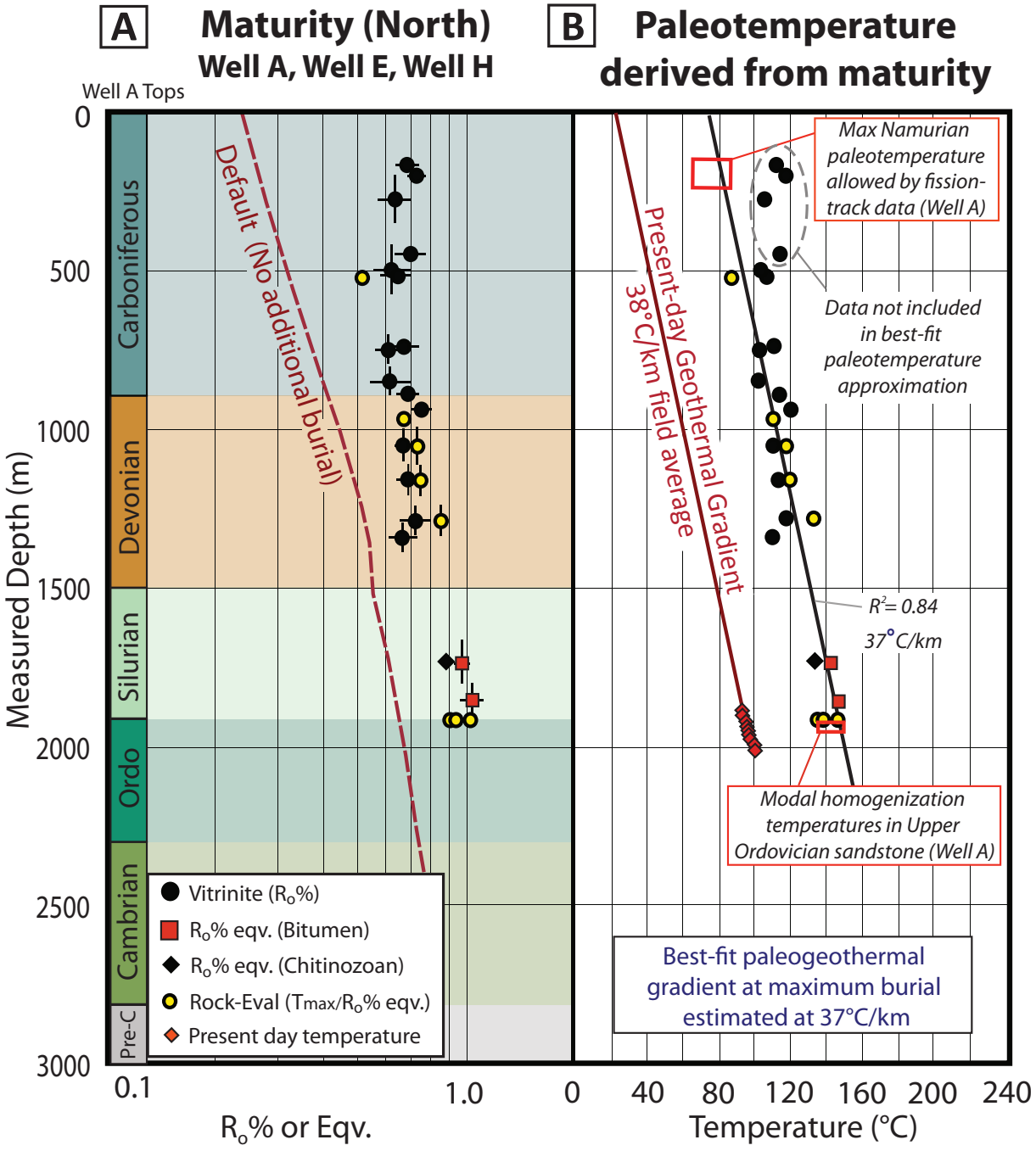
A
Maturity (North)
Well A, Well E, Well H
B
Paleotemperature derived from maturity
Well A Tops
Carboniferous
Devonian
Silurian
Ordo
Cambrian
Pre-C
Default (No additional burial)
Present-day Geothermal Gradient
38°C/km field average
Max Namurian paleotemperature allowed by fission-track data (Well A)
Data not included in best-fit paleotemperature approximation
R²= 0.84
37°C/km
Modal homogenization temperatures in Upper Ordovician sandstone (Well A)
Best-fit paleogeothermal gradient at maximum burial estimated at 37°C/km
Vitrinite (Ro%)
Ro% eqv. (Bitumen)
Ro% eqv. (Chitinozoan)
Rock-Eval (Tmax/Ro% eqv.)
Present day temperature
Measured Depth (m)
0
500
1000
1500
2000
2500
3000
0.1
1.0
Ro% or Eqv.
0
40
80
120
160
200
240
Temperature (°C)

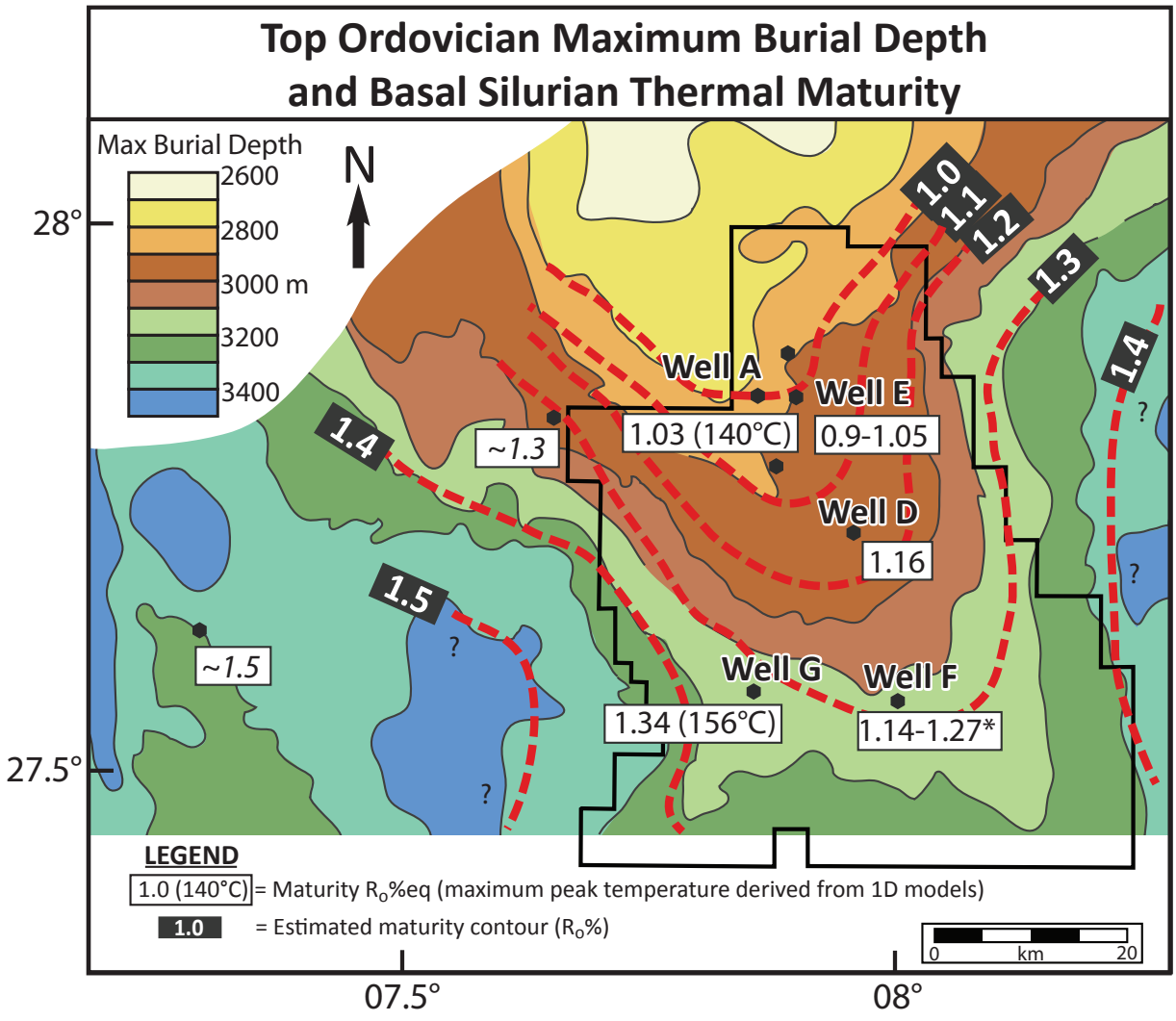
Top Ordovician Maximum Burial Depth
and Basal Silurian Thermal Maturity
Max Burial Depth
2600
2800
3000 m
3200
3400
N
28°
27.5°
07.5°
08°
1.0
1.1
1.2
1.3
1.4
1.4
1.5
Well A
Well E
1.03 (140°C)
0.9-1.05
~1.3
Well D
1.16
~1.5
Well G
Well F
1.34 (156°C)
1.14-1.27*
?
?
?
LEGEND
1.0 (140°C) = Maturity Ro%eq (maximum peak temperature derived from 1D models)
1.0 = Estimated maturity contour (Ro%)
0
km
20

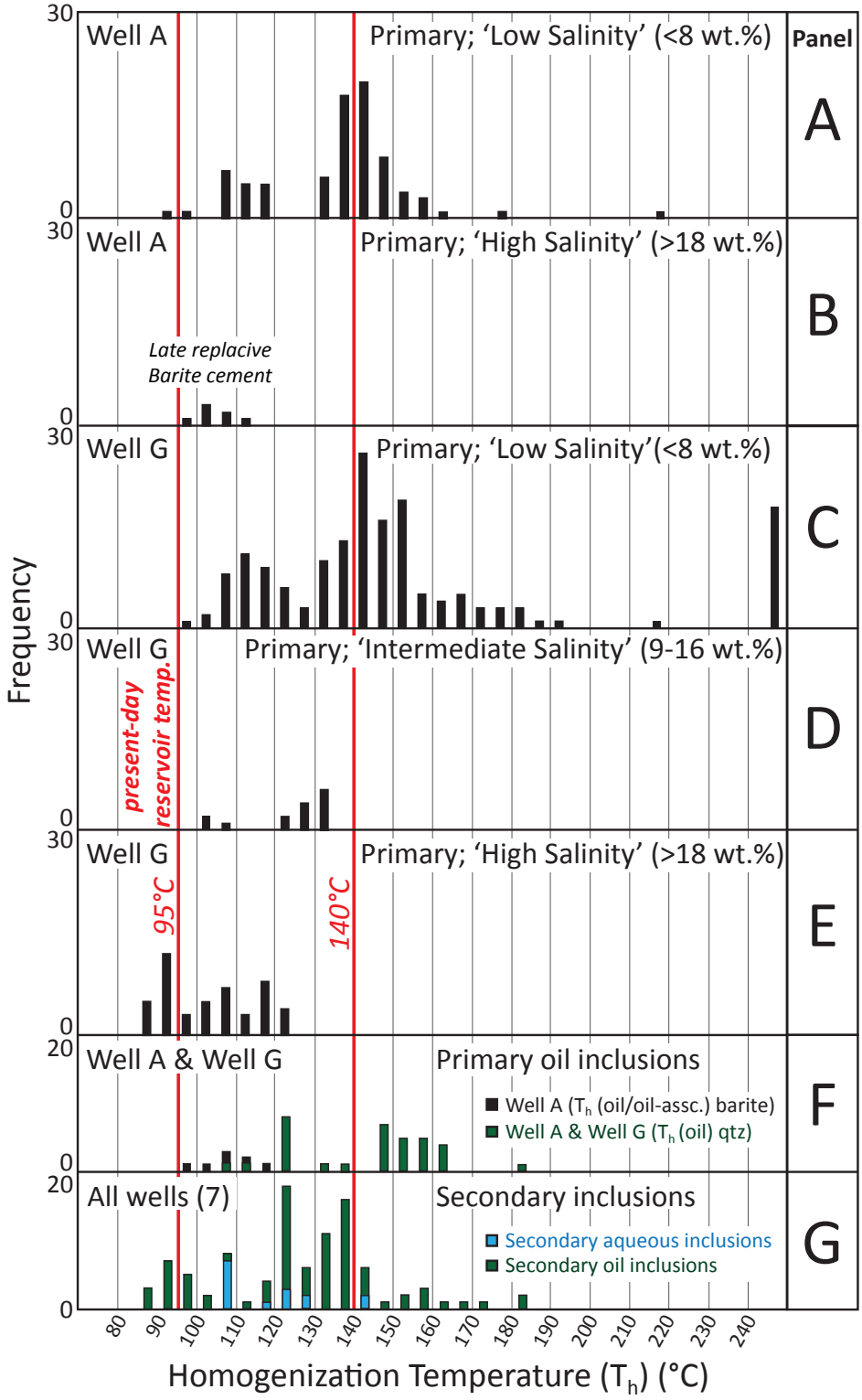
Well A
Primary; 'Low Salinity' (<8 wt.%)
Panel
A
Well A
Primary; 'High Salinity' (>18 wt.%)
Late replacive
Barite cement
B
Well G
Primary; 'Low Salinity'(<8 wt.%)
C
Well G
Primary; 'Intermediate Salinity' (9-16 wt.%)
present-day
reservoir temp.
D
Well G
Primary; 'High Salinity' (>18 wt.%)
95°C
140°C
E
Well A & Well G
Primary oil inclusions
Well A (Th (oil/oil-assc.) barite)
Well A & Well G (Th (oil) qtz)
F
All wells (7)
Secondary inclusions
Secondary aqueous inclusions
Secondary oil inclusions
G
Frequency
Homogenization Temperature (Th) (°C)

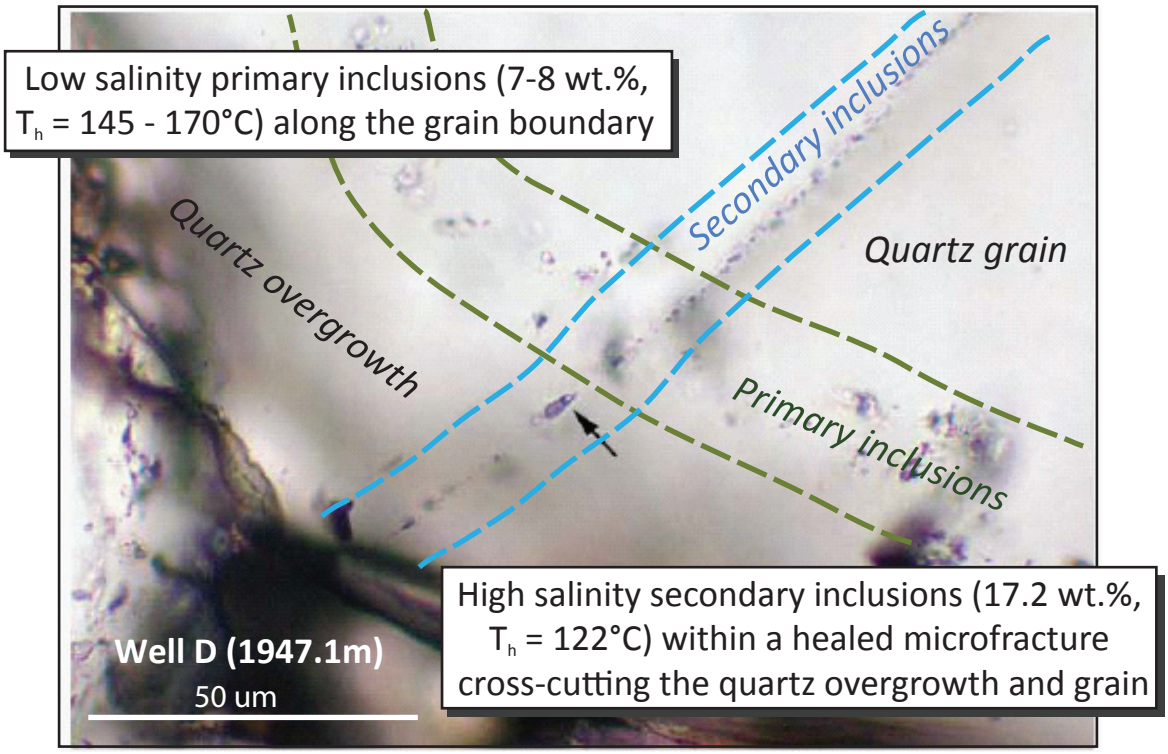
Low salinity primary inclusions (7-8 wt.%, T_h = 145 - 170°C) along the grain boundary
Secondary inclusions
Quartz grain
Quartz overgrowth
Primary inclusions
High salinity secondary inclusions (17.2 wt.%, T_h = 122°C) within a healed microfracture cross-cutting the quartz overgrowth and grain
Well D (1947.1m)
50 um

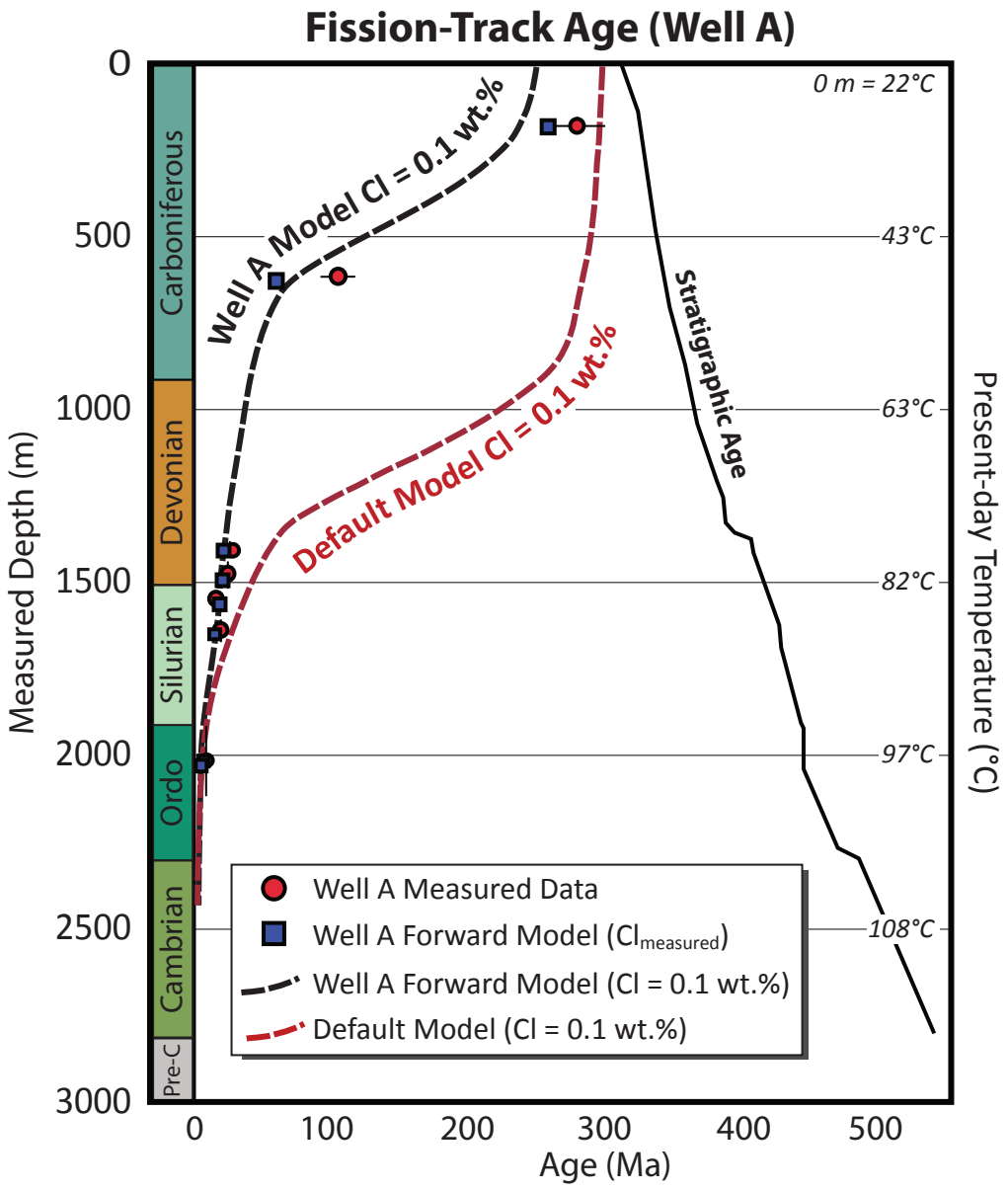
Fission-Track Age (Well A)
0 m = 22°C
43°C
63°C
82°C
97°C
108°C
Well A Model Cl = 0.1 wt.%
Default Model Cl = 0.1 wt.%
Stratigraphic Age
Carboniferous
Devonian
Silurian
Ordo
Cambrian
Pre-C
Well A Measured Data
Well A Forward Model (Cl measured)
Well A Forward Model (Cl = 0.1 wt.%)
Default Model (Cl = 0.1 wt.%)
Measured Depth (m)
0
500
1000
1500
2000
2500
3000
Present-day Temperature (°C)
0
100
200
300
400
500
Age (Ma)

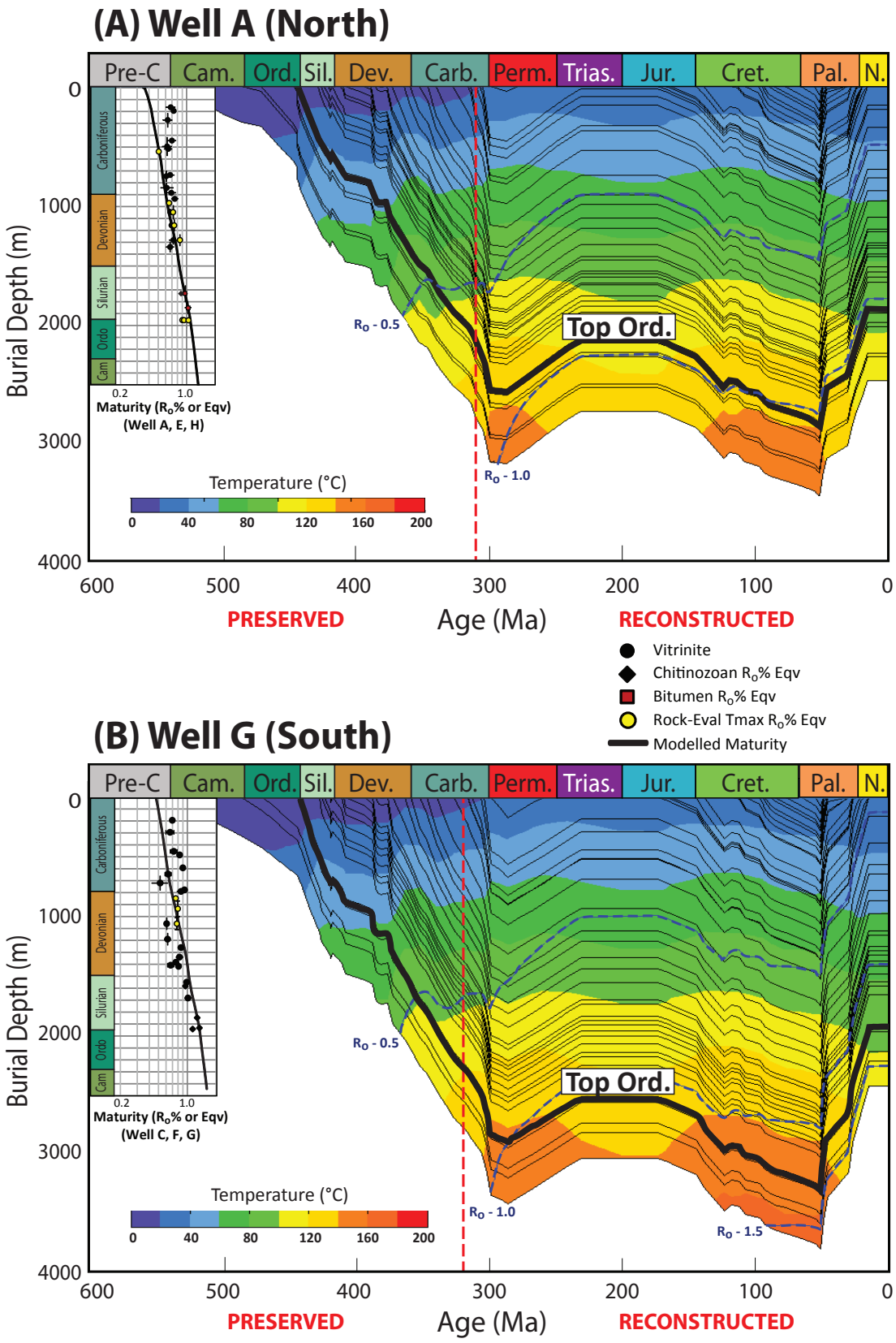
(A) Well A (North)
Pre-C
Cam.
Ord.
Sil.
Dev.
Carb.
Perm.
Trias.
Jur.
Cret.
Pal.
N.
Carboniferous
Devonian
Silurian
Ordo
Cam
0.2
1.0
Maturity (Ro% or Eqv)
(Well A, E, H)
Temperature (°C)
0
40
80
120
160
200
Ro - 0.5
Ro - 1.0
Top Ord.
Burial Depth (m)
0
1000
2000
3000
4000
600
500
400
300
200
100
0
PRESERVED
Age (Ma)
RECONSTRUCTED
Vitrinite
Chitinozoan Ro% Eqv
Bitumen Ro% Eqv
Rock-Eval Tmax Ro% Eqv
Modelled Maturity
(B) Well G (South)
Maturity (Ro% or Eqv)
(Well C, F, G)
Ro - 1.5

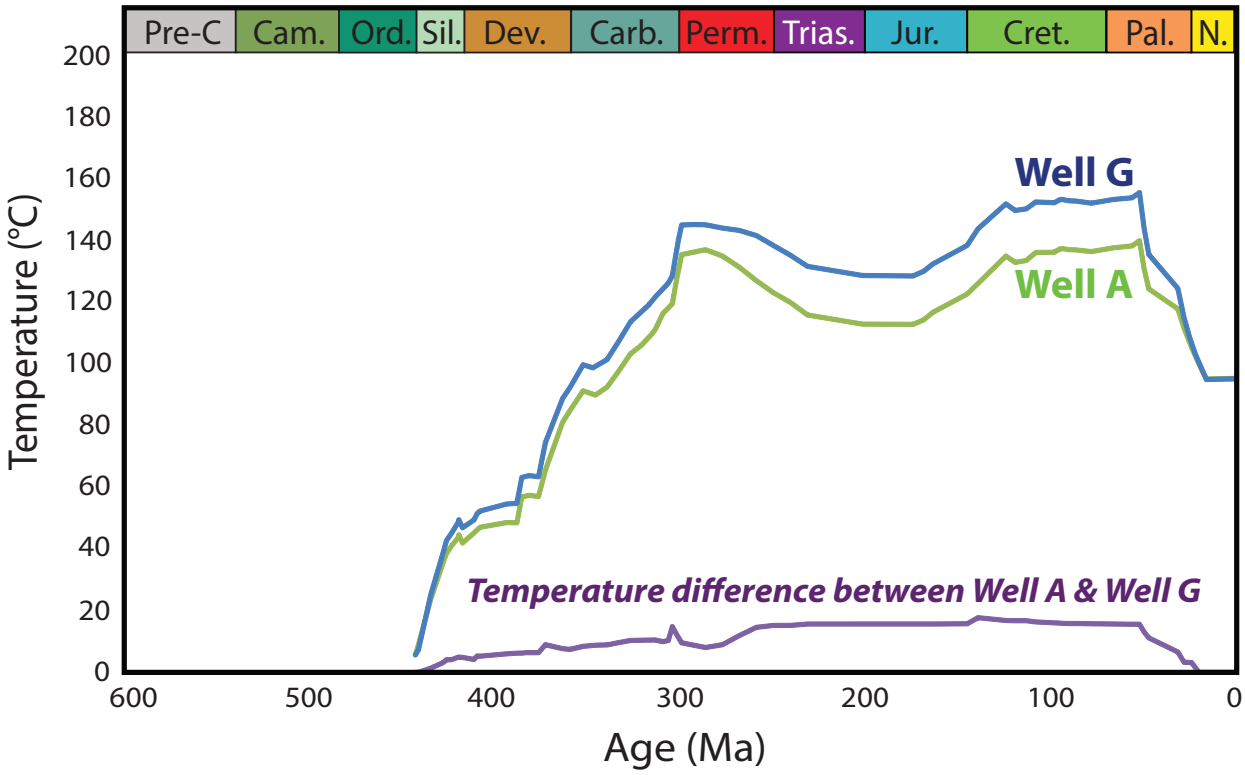
Pre-C
Cam.
Ord.
Sil.
Dev.
Carb.
Perm.
Trias.
Jur.
Cret.
Pal.
N.
Temperature (°C)
200
180
160
140
120
100
80
60
40
20
0
600
500
400
300
200
100
0
Age (Ma)
Well G
Well A
Temperature difference between Well A & Well G

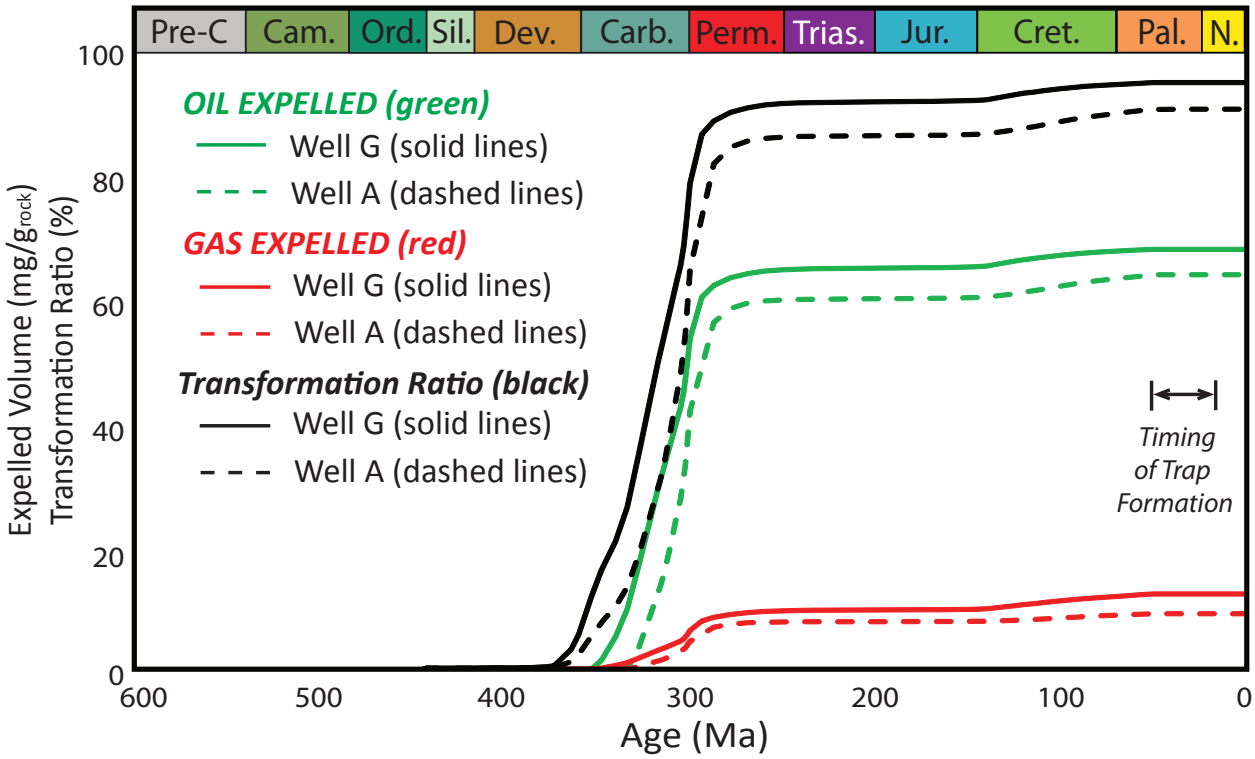
Pre-C
Cam.
Ord.
Sil.
Dev.
Carb.
Perm.
Trias.
Jur.
Cret.
Pal.
N.
OIL EXPELLED (green)
Well G (solid lines)
Well A (dashed lines)
GAS EXPELLED (red)
Well G (solid lines)
Well A (dashed lines)
Transformation Ratio (black)
Well G (solid lines)
Well A (dashed lines)
Timing of Trap Formation
Expelled Volume (mg/g rock)
Transformation Ratio (%)
100
80
60
40
20
0
600
500
400
300
200
100
0
Age (Ma)

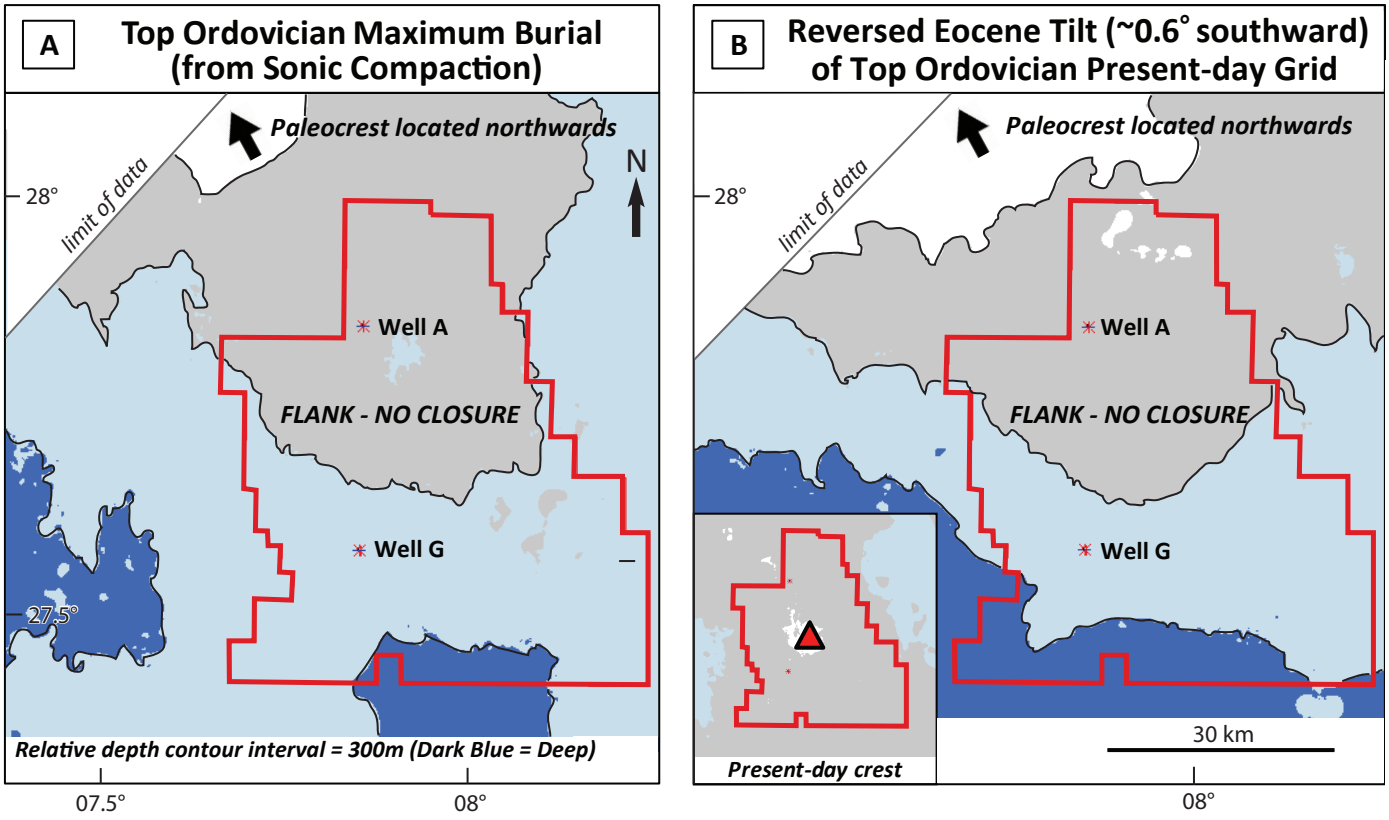
A
Top Ordovician Maximum Burial
(from Sonic Compaction)
Paleocrest located northwards
limit of data
28°
N
Well A
FLANK - NO CLOSURE
Well G
27.5°
Relative depth contour interval = 300m (Dark Blue = Deep)
07.5°
08°
B
Reversed Eocene Tilt (~0.6° southward)
of Top Ordovician Present-day Grid
Paleocrest located northwards
limit of data
28°
Well A
FLANK - NO CLOSURE
Well G
Present-day crest
30 km
08°

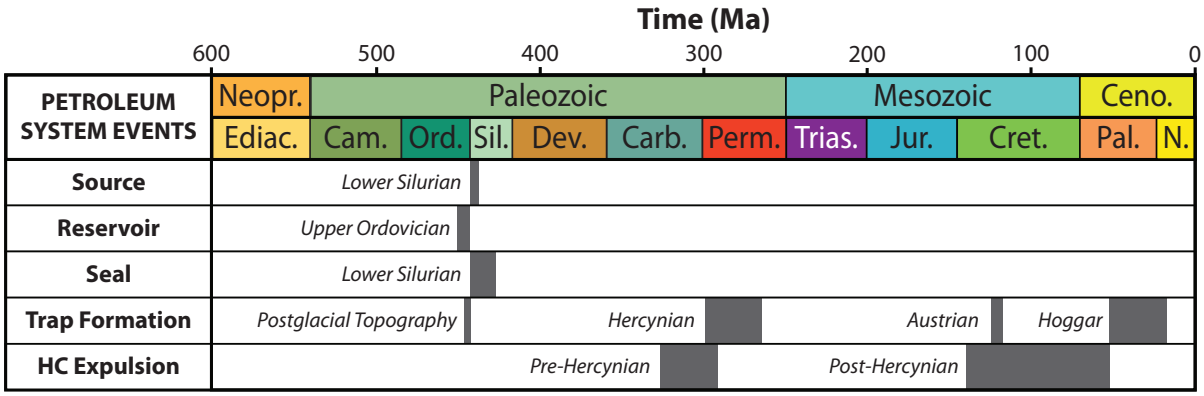
Time (Ma)
600
500
400
300
200
100
0
PETROLEUM SYSTEM EVENTS
Neopr.
Paleozoic
Mesozoic
Ceno.
Ediac.
Cam.
Ord.
Sil.
Dev.
Carb.
Perm.
Trias.
Jur.
Cret.
Pal.
N.
Source
Lower Silurian
Reservoir
Upper Ordovician
Seal
Lower Silurian
Trap Formation
Postglacial Topography
Hercynian
Austrian
Hoggar
HC Expulsion
Pre-Hercynian
Post-Hercynian

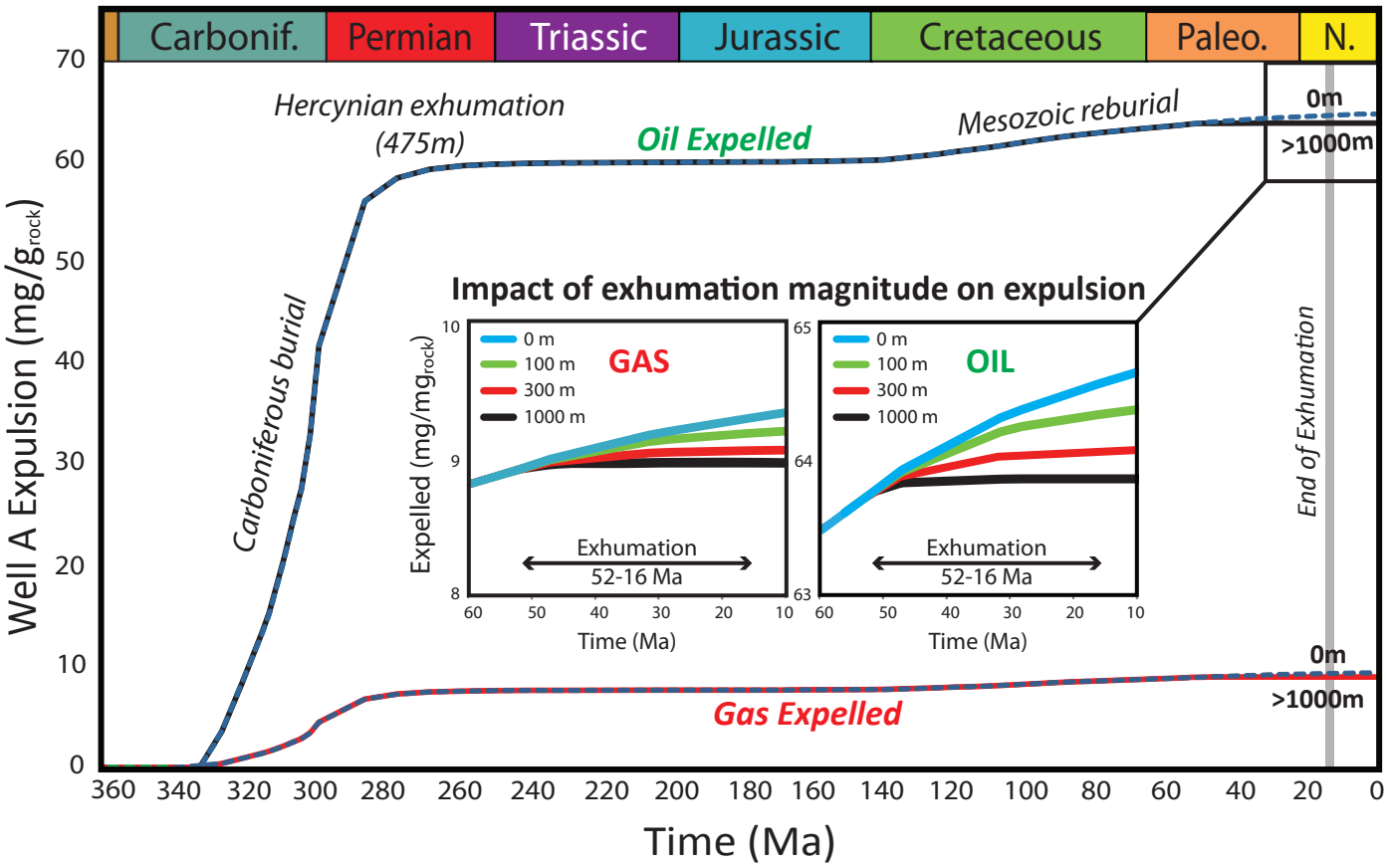
Carbonif.
Permian
Triassic
Jurassic
Cretaceous
Paleo.
N.
Well A Expulsion (mg/g$_{rock}$)
Time (Ma)
Hercynian exhumation
(475m)
Oil Expelled
Mesozoic reburial
0m
>1000m
Carboniferous burial
End of Exhumation
Impact of exhumation magnitude on expulsion
Expelled (mg/mg$_{rock}$)
0 m
100 m
300 m
1000 m
GAS
OIL
Exhumation
52-16 Ma
Time (Ma)
Gas Expelled
0m
>1000m